Molecular Cell

Interferon α/β Enhances the Cytotoxic Response of MEK Inhibition in Melanoma

Graphical Abstract

Authors

Oren Litvin, Sarit Schwartz, ..., Christine Pratilas, Dana Pe'er

Correspondence

dpeer@biology.columbia.edu

In Brief

Litvin et al. developed a computational method to identify targets of MAPK in melanoma and found that most genes are targets only in a subset of cell lines. They showed that interferon plays an important role in response to MAPK inhibition, and that IFNα/β enhances the effect of MEK inhibition.

Highlights

- Most targets of MAPK pathway are regulated by it only in a subset of cell lines

- Cell lines with high activity of IFN pathway are resistant to MEK inhibition

- IFNα/β treatment enhances the cytotoxic response of MEK inhibition

- In resistant cells, CytoC is released but caspases are not cleaved

Accession Numbers

GSE51115

CellPress

Molecular Cell
Article

CellPress

Interferon α/β Enhances the Cytotoxic Response of MEK Inhibition in Melanoma

Oren Litvin,[1] Sarit Schwartz,[2] Zhenmao Wan,[1] Tanya Schild,[1] Mark Rocco,[1] Nul Loren Oh,[1] Bo-Juen Chen,[1] Noel Goddard,[1] Christine Pratilas,[2,3] and Dana Pe'er[1,*]
[1]Department of Biological Sciences and Department of Systems Biology, Columbia University, 1212 Amsterdam Avenue, New York, NY 10027, USA
[2]Program in Molecular Pharmacology and Chemistry
[3]Department of Pediatrics
Memorial Sloan Kettering Cancer Center, New York, NY 10065, USA
*Correspondence: dpeer@biology.columbia.edu
http://dx.doi.org/10.1016/j.molcel.2014.12.030

SUMMARY

Drugs that inhibit the MAPK pathway have therapeutic benefit in melanoma, but responses vary between patients, for reasons that are still largely unknown. Here we aim at explaining this variability using pre- and post-MEK inhibition transcriptional profiles in a panel of melanoma cell lines. We found that most targets are context specific, under the influence of the pathway in only a subset of cell lines. We developed a computational method to identify context-specific targets, and found differences in the activity levels of the interferon pathway, driven by a deletion of the interferon locus. We also discovered that IFNα/β treatment strongly enhances the cytotoxic effect of MEK inhibition, but only in cell lines with low activity of interferon pathway. Taken together, our results suggest that the interferon pathway plays an important role in, and predicts, the response to MAPK inhibition in melanoma. Our analysis demonstrates the value of system-wide perturbation data in predicting drug response.

INTRODUCTION

Advances in the identification and understanding of oncogenic pathways, as well as the development of highly specific drugs, allow clinicians to tailor treatments based on tumor genomics. However, drug response is variable in both experimental systems and in the clinic, even when all tumors harbor mutations that activate the pathways targeted by the drugs (Flaherty et al., 2010; Joseph et al., 2010; Pratilas et al., 2009; Slamon et al., 2001).

Here, we focus on the variability in response to ERK-MAPK pathway inhibition in melanoma. At least 70% of melanoma tumors harbor an oncogenic mutation in the ERK-MAPK pathway (Hodis et al., 2012), and drugs targeting this pathway have been approved with observed clinical success (Sosman et al., 2012). However, phenotypic responses to MAPK pathway inhibitors,

both in patients and in vitro, vary dramatically (Flaherty et al., 2010; Joseph et al., 2010).

Several molecular mechanisms have been proposed to explain response heterogeneity. Feedback reactivation of the pathway attenuates the inhibitory effects of the drugs (Lito et al., 2012; Poulikakos et al., 2010). Other studies found *PTEN* and *MITF* status correlated to response heterogeneity (Johannessen et al., 2013; Paraiso et al., 2011; Xing et al., 2012), but these explain only part of the observed variability. While these factors may contribute to the heterogeneous response, they are limited by characterizing the overall phenotypic response, without distinguishing cytotoxic from cytostatic phenotypes.

We aim to explain the phenotypic variability in response to MAPK inhibition by studying the transcriptional response to this inhibition. While most studies use correlation between genetic and genomic features and phenotypic outcome to identify predictive features (Barretina et al., 2012; Garnett et al., 2012), we take a different approach. We use pre- and post-MEK inhibition expression data in a panel of genetically diverse cell lines to get a better understanding of the targets and pathways regulated by ERK-MAPK, and use these regulation patterns, and how they differ between tumors, to explain the variability in response to treatment. In this study, genes with changes in their mRNA levels following MEK inhibition are defined as targets of the MAPK pathway.
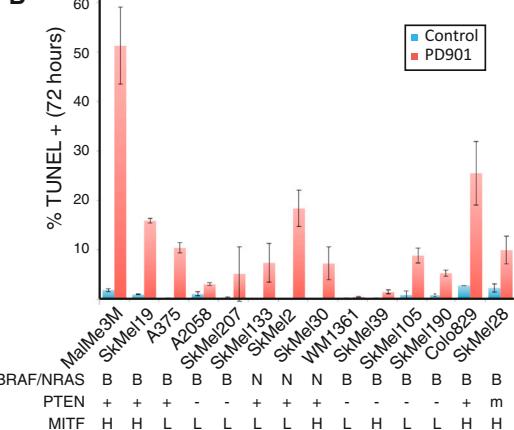
We found extensive heterogeneity in the transcriptional response to MEK inhibition between cell lines. Although all cell lines harbor a MAPK pathway activating mutation (either NRAS or BRAF), a vast majority of MAPK targets are context-specific, under the control of the pathway in only a subset of cell lines (hereafter, a *context* refers to any subset of the cell lines, with or without a known, shared, and unique genetic feature). As these differences could reveal the molecular mechanisms underlying phenotypic variance, we developed a computational tool, *context-specific regulation* (COSPER), to identify context-specific targets using pre- and postperturbation gene expression data.

Analysis with COSPER revealed that the IFN-type I pathway presents context-specific behavior. While studying this pathway, we found that type I interferon (IFNα/β) strongly enhances the cytotoxic response of MEK inhibition. We show that cell lines
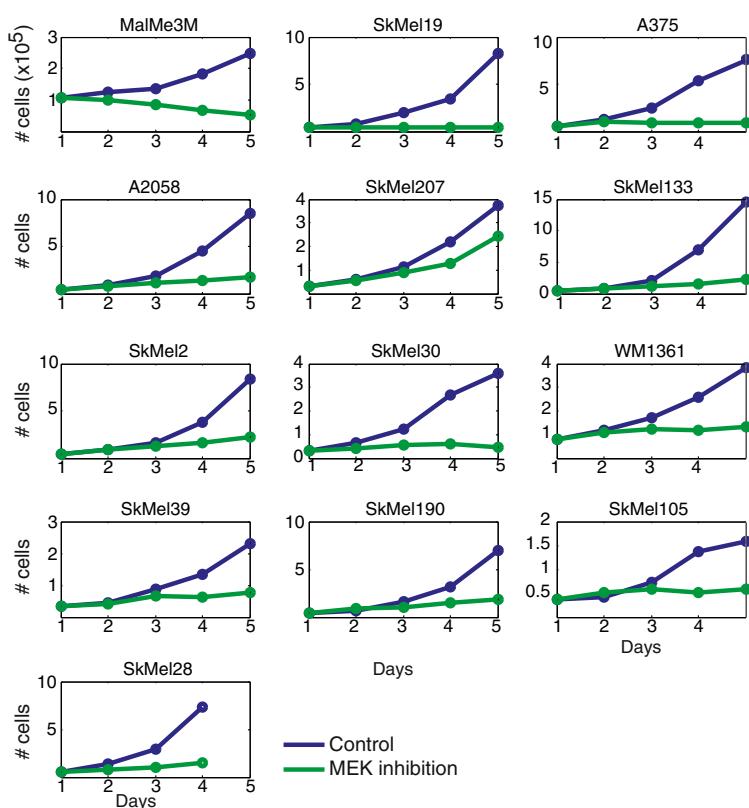
Figure 1. Phenotypic Heterogeneity in Response to MEK Inhibition in Melanoma

(A) BRAF, NRAS, *PTEN*, and *MITF* status show the genetic diversity of our panel of 14 cell line panel. We used 50 nM of PD325901 that fully inhibits the pathway in both NRAS and BRAF mutant cell lines (Figure S1A).

(B) Mean percentage ± SD of TUNEL+ cells after 72 hr of treatment with DMSO (control) or PD901 (50 nM). MAPK mutation, *PTEN* status, and *MITF* status are listed at the bottom.

(C) Growth curves of untreated (blue) and MEK-inhibited (green) cells showing variation in response.

with high basal activity of the interferon pathways are resistant to MEK inhibition alone or its combination with IFNα/β. We identified that a deletion of the interferon locus is correlated with basal activity level of the interferon pathway and predicts the cytotoxic response of MEK inhibition.

Our results demonstrate that inhibition of a key oncogenic pathway leads to substantially different transcriptional programs in different cell lines. We show that a better understanding of the interactions and activity state of different pathways would enable clinicians to tailor new and unexpected drug combinations to individual patients, which may lead to better clinical responses.
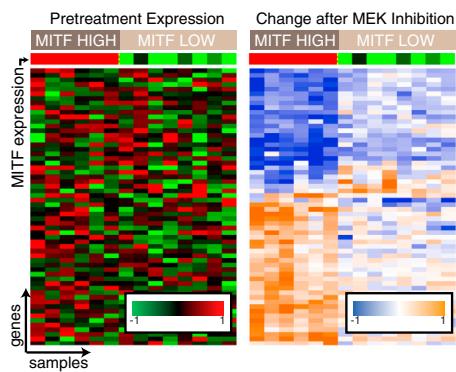
RESULTS

Cell lines harboring MAPK-activating mutations vary in their response to inhibition of the pathway, both in rate of proliferation and death (Xing et al., 2012). To characterize the targets and crosstalk of the ERK-MAPK pathway, we chose a panel of 14 genetically diverse melanoma cell lines. This panel represents the spectrum of common genetic aberrations in mel-

anoma—MAPK mutations, *MITF* amplification, and *PTEN* deletion (Figure 1A).

We compared the transcriptional and phenotypic response to MAPK pathway inhibition of both NRAS-mut and BRAF-mut cell lines using a MEK inhibitor (PD325901, 50 nM) that fully inhibits the pathway in all cell lines at 8 hr (see Figure S1A available online), and not the clinically used BRAF inhibitor, which works on BRAF-mut cells only. A comparison of the MEK inhibitor with a BRAF inhibitor (PLX4720; Tsai et al., 2008) in a BRAF-V600E cell line shows almost identical transcriptional response, both in the genes affected and in the extent of transcriptional change (see Supplemental Information and Figure S1B for more information).

We first characterized the cell lines' phenotypic responses to MEK inhibition. The cell lines display a wide range of cytotoxic responses, as well as differences in proliferation under MEK inhibition (Figures 1B and 1C). Notably, and contrary to previously published results (Barretina et al., 2012; Xing et al., 2012), we found that key genetic aberrations common in melanoma, including *MITF* and *PTEN* status, and MAPK mutation type, fail to fully explain the response heterogeneity (Figures 1B, S1C, and S1D).

A Perturbation reveals heterogeneity

B Context-specific transcriptional targets of MAPK

C Number of genes with a fold change >= X in Y or more cell lines

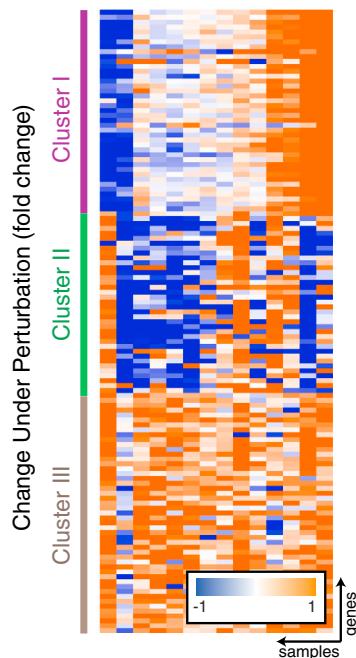| Fold change \ Cell lines	1	4	7	10	14
2	3386	936	432	165	18
4	776	137	55	29	4
8	233	36	14	5	2
16	83	12	7	2	1

Figure 2. Transcriptional Heterogeneity in Response to MEK Inhibition in Melanoma

(A) MEK inhibition reveals transcriptional targets of MEK (right), undetectable in steady-state conditions (left). These genes are only regulated by MEK in high-*MITF* cell lines. In this and other heatmap figures, columns are samples, and rows are genes. Red-black-green plots represent pretreatment levels comparing between cell lines, and orange-white-blue plots show expression fold change 8 hr after treatment (both in log2 scale). The same genes (in the same order) are shown in both heatmaps; Table S1 lists the genes in the figure.

(B) Three gene clusters demonstrating the extent of context specificity of MAPK targets. In each of the three clusters, cell lines show a different response to MEK inhibition. Moreover, each cell line is unique, and responses for each cell lines are different in each cluster.

(C) Number of differentially expressed genes as a function of fold change and number of cell lines. Arbitrarily choosing the cutoff is likely to mislabel hundreds of genes. BRAF and *PTEN* status are not correlated with transcriptional response to MEK inhibition (Figure S2).

Heterogeneity in Transcriptional Response to MAPK Inhibition

To identify MAPK transcriptional targets and how these differ across cell lines, we characterized the transcriptional response before and after MEK inhibition. We measured gene expression 8 hr following MEK inhibition to capture the peak of the transcriptional changes following inhibition (Pratilas et al., 2009).

Our data show that MEK inhibition reveals transcriptional patterns that are not observable in steady state expression—genes that display no correlation in their gene expression levels before pathway inhibition—become strongly correlated following MEK inhibition. In Figure 2A (list of genes in Table S1) we see a set of genes that are only correlated in the context of *MITF* levels in their transcriptional response to MEK inhibition. These same genes show no correlation between themselves and with *MITF* levels in their baseline, preinhibition levels. Their association with *MITF* can therefore only be revealed when measuring their postperturbation response. We found this phenomenon widespread with almost 4,000 genes that behave in concert only after perturbation (full details in Supplemental Information).

The most striking phenomenon observed in postinhibition data is the heterogeneity in response to MEK inhibition across different cell lines. Although all cell lines harbor a MAPK-activating mutation, most genes are regulated by the MAPK pathway in only a subset of the cell lines, and no two cell lines behave similarly (Figure 2B). For example, only 18 genes change by >2-fold in all 14 cell lines, but 936 genes pass this threshold in four or more cell lines (Figure 2C). We term those genes *context-specific targets*—under the control of the MAPK pathway in only a subset of cell lines. The term "context" is used to represent a known or unknown genetic or genomic background that is shared by a subset of cell lines, but not by the others. Notably, we didn't find a significant enrichment of genes regulated by MAPK only in BRAF-mut or NRAS-mut cell lines (Figures S2A and S2B).

Our data show that MEK inhibition leads to different phenotypic responses in different cell lines, and that MAPK regulates different genes, and presumably different pathways, in different cell lines. We hypothesized that that differential regulation of pathways and genes underlies the phenotypic variability, and that identifying context-specific targets might explain it. Therefore, we investigated the patterns of context-specific regulation.

Context-Specific Regulation

The first step in the analysis was to identify targets of the MAPK pathway using postinhibition changes in expression levels. However, Figure 2C shows that choosing an arbitrary fold change threshold and number of tumors to classify genes as targets and nontargets can lead to misclassification. We therefore developed a method that specifically searches for context-specific MAPK regulated genes using both pre- and postperturbation data.

At the core of our method is the observation that some genes show distinct patterns of context-specific regulation both before and after MAPK inhibition. *HEY1* is used as an example of a context-specific regulated gene (Figure 3A). *HEY1* has two states, or contexts, that are detectable in both pre- and postinhibition expression levels. In one context (i.e., one set of cell lines) it is not under the control of MAPK, and shows low basal
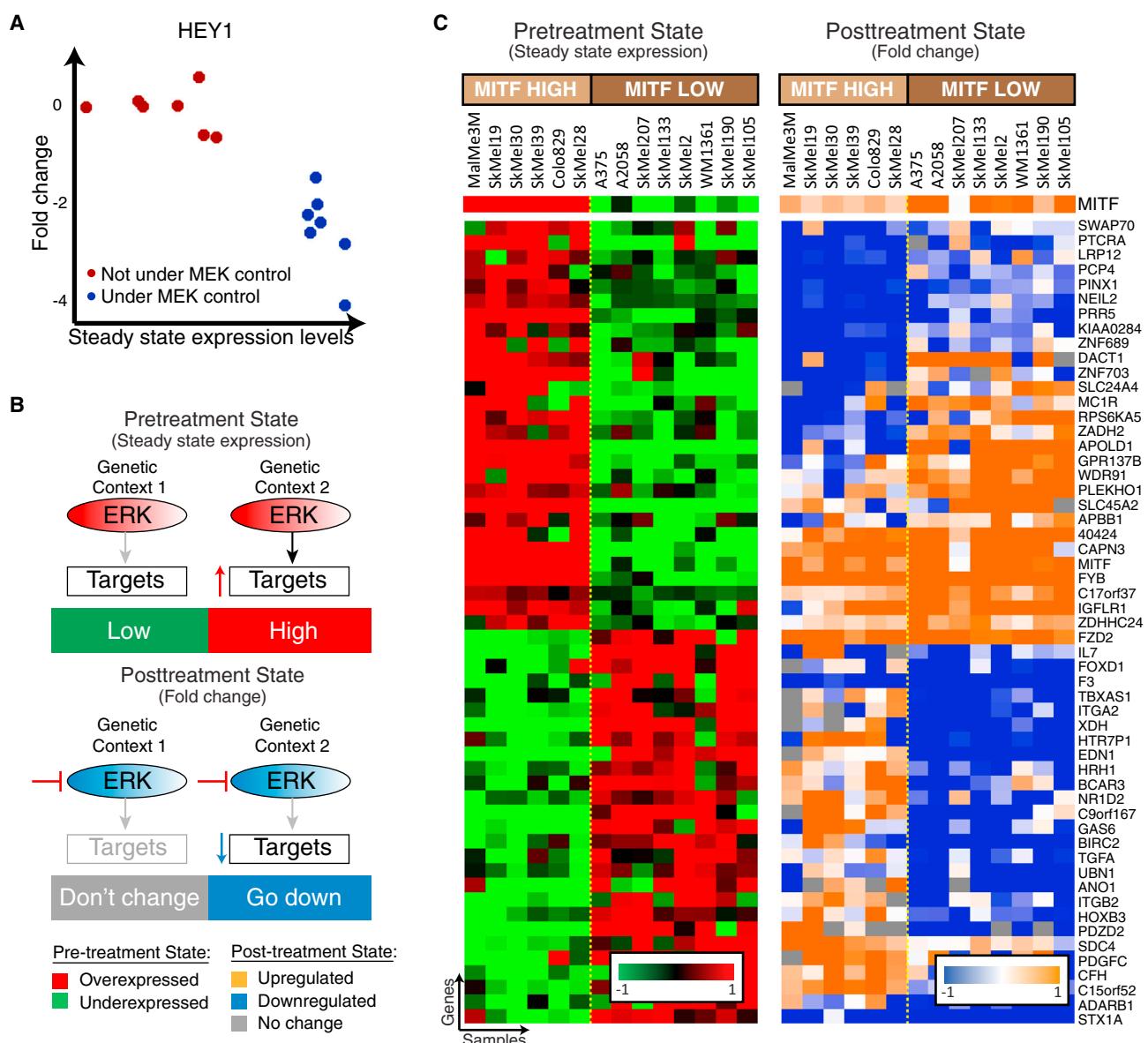
Figure 3. COSPER Identifies COntext-SPEcific Regulation—Genes Are under the Control of MAPK in Only a Subset of Cell Lines, Both Before and After Inhibition

(A) HEY1 is an example for a context-specific target, regulated by MAPK in only a subset of cell lines (blue dots). MEK inhibition doesn't affect its expression in the other group of cells (red), and its basal expression is lower in these cell lines.

(B) A cartoon of context-specific regulation exhibited by *HEY1*. ERK upregulates a set of targets only in genetic context 2, while it has no effect in the context 1 (upper panel). Therefore, the genes are downregulated following MEK inhibition only in genetic context 2 (lower panel).

(C) COSPER identifies gene clusters with context-specific regulation. The cluster contains genes controlled by MAPK only in cell lines with high-MITF mRNA expression. *MITF* expression, which is not part of this cluster, is in the top row. Several patterns of regulation (up- and downregulation) are shown.

expression levels when MAPK is active, and its expression doesn't change after inhibition of the pathway (Figure 3A, red dots). In the second group of cell lines (blue dots), *HEY1* is upregulated by MAPK and therefore shows high basal expression levels before pathway inhibition, and its expression drops following MEK inhibition.

As genes are often coregulated, we expect clusters of context-specific coregulated genes (Figure 3B). Using clusters of genes

to identify contexts and context-specific targets enables us to computationally reduce the experimental noise, and increase the probability that the association between a context and a gene is a product of an underlying biological phenomenon rather than a spurious association.

We developed a computational method—COSPER—that uses pre- and postinhibition transcriptional data to identify context-specific coregulated clusters of genes.

COSPER Identifies Context-Specific MAPK-Regulated Genes

COSPER can be viewed as a biclustering algorithm, designed to identify gene clusters that show context-specific regulation patterns (Figure 3B). In each cluster, the cell lines are divided into two groups, or *contexts*, and the genes have a distinct but different behavior in each context, both before and after pathway inhibition. Combining data from both pre- and postpathway inhibition focuses the search to genes that are likely to be regulated by the MAPK pathway. By identifying the genes regulated by the pathway in only a subset of cell lines, e.g., sensitive versus resistant, COSPER helps focus the analysis on genes and pathways that are likely to contribute to the phenotypic response to pathway inhibition.

COSPER is not restricted to the patterns depicted in Figure 3A, and can identify any context-specific pattern of regulation (Figure 3C). Overall, COSPER identified 70 context-specific clusters with five genes or more, and assigned a total of 1,024 genes to clusters (genes are allowed to belong to more than one cluster; list of all clusters appears in Table S2; for full algorithmic detail, see Supplemental Information). Fifteen clusters associate with *MITF*, containing 401 genes in total. These clusters either have a perfect correlation with *MITF* expression, such as the cluster in Figure 3C, or have one to two cell lines that "switch sides"—they behave similarly to cell lines with the opposite *MITF* status (Figures 4A and S3A, which include *HEY1*).

Notably, none of the clusters correlate with the oncogenic activation of MAPK (BRAF or NRAS), or with the cells' *PTEN* status. Moreover, we also explicitly tested for genes correlated with these aberrations, but no gene's expression was found to be significantly associated with these mutations (see Supplemental Information and Figure S2).

Inferring Pathway Activity Using COSPER

COSPER identifies clusters of genes downstream of MAPK that show context-specific behavior. Using standard gene set enrichment analysis methods, we can postulate the pathways that govern the differential expression of those genes, and the activity of the clusters' regulators.

For example, the clusters in Figures 3C and 4A demonstrate the different roles of MITF isoforms. While the cluster in Figure 3C correlates with *MITF* mRNA expression, the cluster in 4A correlates with the abundance of the MITF-M protein isoform (Figure 4B). MITF itself is also regulated by MAPK, both at the mRNA and protein levels (Figures S3B and S3C).

The different functional annotations of the genes in the two clusters suggest that different MITF isoforms regulate different processes. The promoters for genes in the MITF-M cluster are highly enriched for the MITF binding site (CACATG) (Levy et al., 2006) (p value = 10^{-3} compared with 0.7 for genes in MITF-expression cluster; see Supplemental Information for details). However, the *MITF*-expression cluster, but not the MITF-M cluster, is enriched for the GO annotation "melanocyte differentiation" (q value = 10^{-4}), suggesting that another isoform of MITF is responsible for cellular differentiation.

An additional cluster COSPER identified is correlated with STAT3 activity (Figures 4C and S3D). Gene ontology enrichment analysis found that the genes in the cluster are enriched for *cyto-kine-cytokine receptor pathway* (q value < 10^{-3}), and with *miR-19* and *miR-17* (q value < 10^{-3}), two miRs known to be regulated by pSTAT3 (Dai et al., 2011; Zhang et al., 2012), which led us to suspect that this cluster is associated with STAT3 regulation. We confirmed these predictions by measuring STAT3 activity in the cell lines. Levels of pSTAT3-Y705, an indicator for STAT3 activity, but not of pSTAT3-S727, match the cluster's contexts (Figures 4D and S3E).

Using the MITF and STAT3 examples, we showed that by combining information from both steady-state and postperturbation data, COSPER infers both network state and interactions between pathways. However, when running COSPER on each data set alone, the resulting clusters are much larger, less specific, and therefore less informative than the clusters resulting from using both conditions (for full comparison analysis, see Supplemental Information). Steady-state data give a point of reference and provide information on basal pathway activation state, while postinhibition data enables the identification of genes directly regulated by the MAPK pathway. Therefore, only by using both data sets does COSPER identify the state and interconnectivity of pathways.

Interferon-STAT1 Pathway Is Differentially Regulated in Cell Lines

COSPER also identified a cluster that contains several interferon targets, *IRF7*, *IRF9*, *CCL5*, and *IFI44L* (Figure 5A), which reflect the activity of the type I interferon pathway (Hecker et al., 2013). Since type I interferon (IFNα/β) is one of the few approved drugs for metastatic melanoma, we decided to focus on this cluster.

The cluster splits the cell lines into two groups; the first contains three cell lines with an upregulation of interferon response genes, and cell lines in the second context express these genes at lower levels. Levels of pSTAT1-Y701, an indicator of the interferon-STAT1 activity levels (Platanias, 2005), confirmed that the high basal expression levels of the pathway targets correspond with high signaling activity of the pathway (Figure 5B). Notably, the cell lines with upregulation of the STAT1-interferon response genes are not the same three cell lines with low activity of STAT3.

High basal activity of the STAT1-interferon pathway has been previously shown to be necessary, but not sufficient, for IFNα/β-induced apoptosis (Jackson et al., 2003). To test this claim, three low- and three high-pSTAT1 cell lines were treated with IFNβ, and apoptosis levels were assessed by TUNEL. All low-pSTAT1 and two high-pSTAT1 cell lines were resistant to the cytotoxic effects of IFNβ, and one high-pSTAT1 cell line was marginally sensitive (Figure 5C). Both IFNα and IFNβ were tested, and as previously shown (Leaman et al., 2003), IFNβ led to a stronger apoptotic response than IFNα (Figure S4A); thus, IFNβ was chosen for further analysis. Our results confirmed the previous findings that STAT1 activity is necessary, but not sufficient, for IFNα/β sensitivity.

IFNβ Enhances the Cytotoxic Response of MEK Inhibition in Low-pSTAT1 Cell Lines

According to the expression data, MEK inhibition leads to an up-regulation of the IFNα/β pathway. Analysis of protein levels by western blots indicates an increase in pSTAT1 levels after MEK
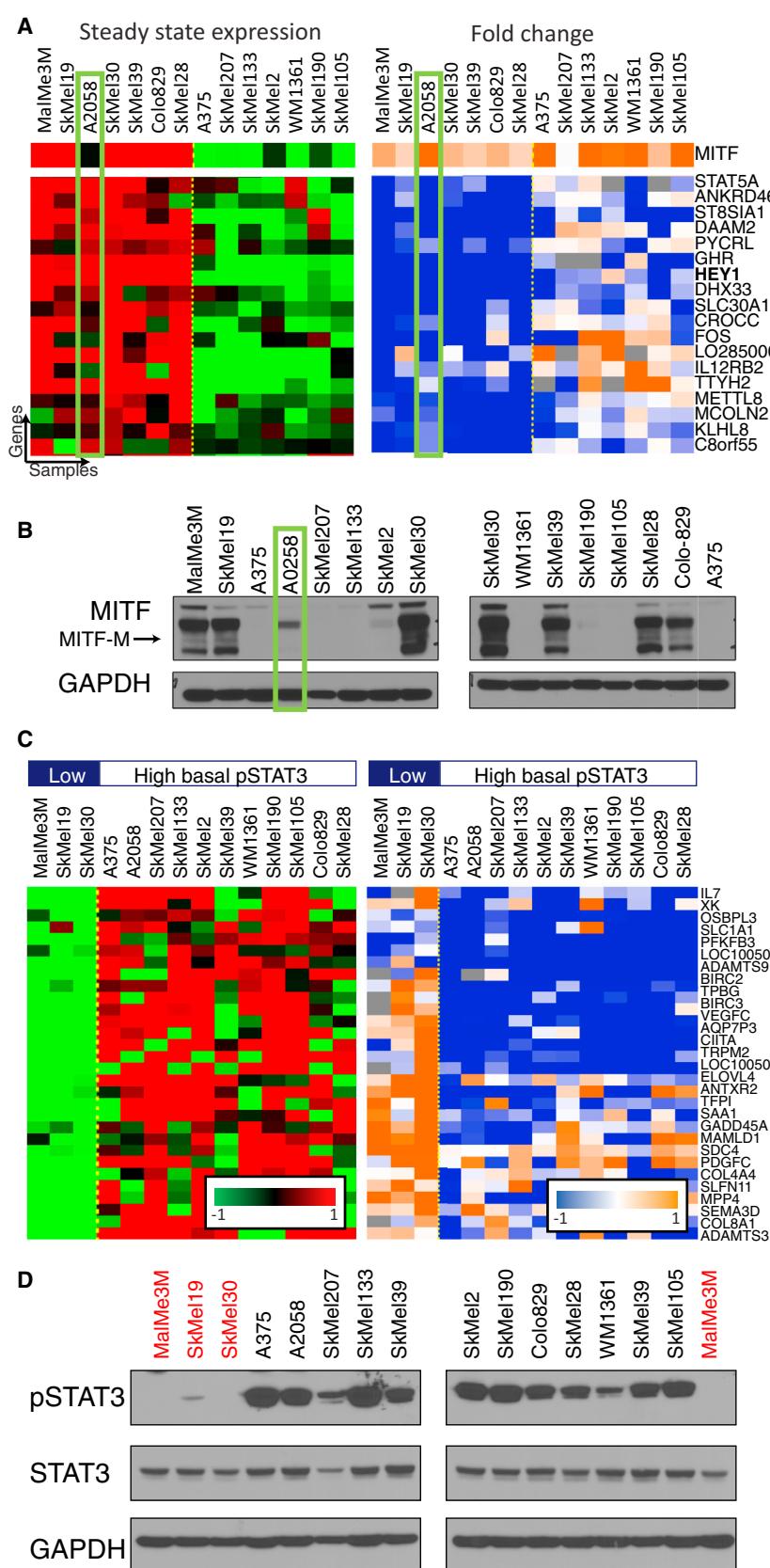
CellPress

Figure 4. Analysis of the Clusters' Genes Facilitates the Identification of Pathways that Exhibit Context-Specific Interactions with the MAPK Pathway

(A) A cluster associated with MITF-M protein levels identified by COSPER. Its genes are overexpressed in high-MITF-M cell lines and are downregulated only in these cells after MEK inhibition. *MITF* expression is in the top row. The cluster is almost perfectly correlated with *MITF* expression, except for one cell line highlighted in green. The binding site of MITF is overrepresented in the promoters of the cluster genes (p value = 10^{-3}). Only part of this cluster's genes is shown (full cluster appears in Figure S3A).

(B) MITF protein levels in all 14 cell lines. A2058 (green rectangle) is the only low mRNA-*MITF* cell line that expresses the MITF-M isoform.

(C) Additional cluster identified by COSPER. The cluster's genes are enriched for STAT3-related GO annotations (full cluster appears in Figure S3D). A bar indicating pSTAT3 levels appears in top row.

(D) As predicted by COSPER, pSTAT3-Y705 levels are correlated with the cluster. Cell lines with low-pSTAT3 are marked in red, matching the first three pSTAT3-low cell lines shown in (C).
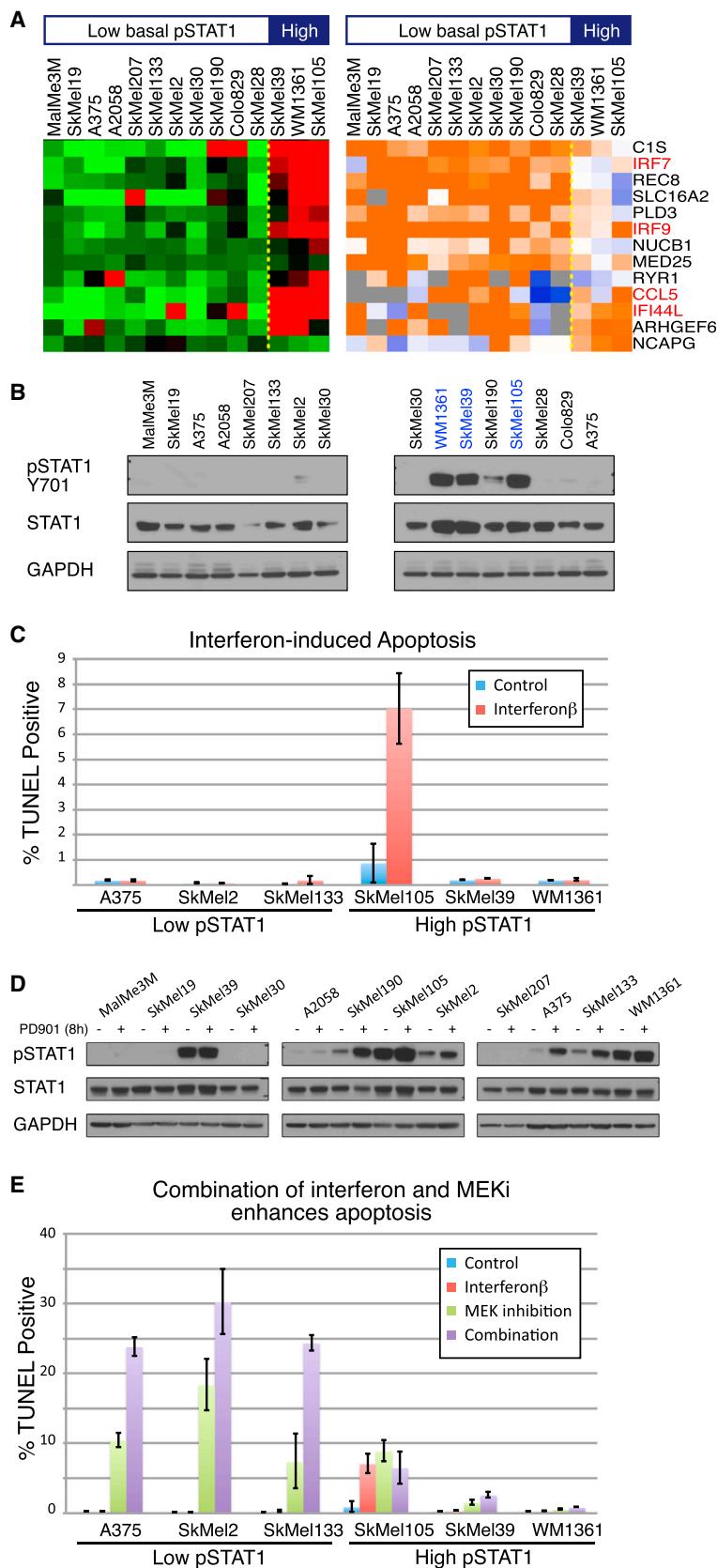
Figure 5. IFNβ Enhances Cytotoxic Response of MEK Inhibition in Low-pSTAT1 Cell Lines

(A) COSPER identified a cluster containing several known interferon targets (marked in red). Three cell lines have high target expression, and MEK inhibition upregulates the pathway in the other 11 cell lines. A bar indicating pSTAT1 levels at the top and these are different than the high-pSTAT3 cell lines of Figure 4.

(B) pSTAT1-Y701, a marker for interferon-STAT1 pathway activity, is correlated with the gene expression and shows high basal activation level in the three high cell lines (blue).

(C) High interferon pathway activity is necessary, but not sufficient, for IFN-induced death. We used TUNEL staining as a marker for apoptosis 72 hr after IFNβ treatment (mean levels ± SD). Only one out of three high-pSTAT1 cell lines respond to IFNβ (red) and none of the low-PSTAT1 lines respond to IFNβ. We used IFNβ, and not IFNα, due to its higher efficacy (see Figure S4A).

(D) MEK inhibition leads to upregulation of pSTAT1 in all cell lines.

(E) MEK inhibition induces death in low-pSTAT1 cell lines only (green). IFNβ dramatically enhances the cytotoxic effect of MEK inhibition in low-pSTAT1 cell lines (purple). High-pSTAT1 cell lines show only mild response to the MEK inhibitor and its combination with IFBβ (right). IFNβ alone (red) has almost no cytotoxic response.

inhibition, confirming a crosstalk between MAPK and STAT1 (Figure 5D). Because interferon activity seems to be required for IFN-induced death, we hypothesized that IFN might synergize with MEK inhibition to increase apoptosis.

The cytotoxic effect of MEK inhibition on both high- and low-pSTAT1 cell lines was assessed. We found that high-pSTAT1 cell lines are mostly resistant to the cytotoxic effects of MEK inhibition, while low-pSTAT1 cells are sensitive (Figure 5E). Notably, both groups contain NRAS and BRAF mutant cell lines and cell lines with high and low *MITF* expression, although both *MITF*-low cell lines and NRAS mutant cell lines have been previously reported to be less sensitive to MAPK pathway inhibition (Barretina et al., 2012; Solit et al., 2006). Moreover, the results show that the cytotoxic response of MEK inhibition is independent of its cytostatic response. For example, SkMel133 continues to grow rapidly under MEK inhibition (Figure 1C) but has relatively high apoptosis levels under MEK inhibition.

We then examined the cytotoxic effect of the combination of MEK inhibition and IFNβ. While IFNβ as a single agent has no cytotoxic effect on low-pSTAT1 cell lines, it notably enhances the cytotoxic response of MEK inhibition, increasing TUNEL-positive cells by almost 2-fold (Figures 5E and S4B). Moreover, while low-pSTAT1 cell lines show a strong sensitivity to the combination of MEK inhibition and IFNβ, high-pSTAT1 cell lines seem to be resistant to the cytotoxic effects of both MEK inhibition alone and the dual treatment (Figure 5E). To confirm that the effect of IFNβ on the cytotoxic response of MAPK pathway inhibition is not specific to MEK inhibition, we show a similar behavior, albeit slightly weaker, between a BRAF inhibitor (PLX4720) and IFNβ (Figure S4C).

Transcriptional Response to IFN Is Similar in All Cell Lines

Our data demonstrated that basal activation level of the interferon pathway predicts the cytotoxic response to MEK inhibition. We hypothesized that these phenotypic differences are associated with changes in the interferon pathway and its response to IFNα/β treatment. We therefore characterized the signaling and transcriptional responses to IFNβ and MEK inhibition.

Western blots show that activation of STAT1 by IFNβ is identical, in both timing and extent, in a low-pSTAT1 cell line and a high-pSTAT1 cell line, and inhibition of MEK does not alter this response (Figures 6A and S5A). Interestingly, we found that the levels of pSTAT1 in the so-called "high-pSTAT1 cell lines" are substantially lower than pSTAT1's levels following IFNβ treatment (compare Figure 6A with Figure 5B).

To search for more global regulatory differences in the interferon response, and to assess the effects of IFNβ more quantitatively, we measured gene expression levels 8 hr after treatment with PD325901, IFNβ, or their combination in three low- and three high-pSTAT1 cell lines (Figure S5B). No significant differences in the transcriptional response following the treatments are apparent after 8 hr of treatment. Additionally, MEK inhibition does not alter the IFNβ response, and no synergy between treatments is revealed (see Supplemental Information and Figure S5C).

These data suggest that the differences in the phenotypic response are not due to the basal activation level of the interferon pathway.

The Caspase Pathway Is Only Activated in Low-pSTAT1 Cell Lines

Since the transcriptional response to IFNβ fails to explain the differences in the cytotoxic response between the cell lines, we moved to characterize the apoptotic pathway directly.

The intrinsic apoptotic pathway is initiated by the release of cytochrome *c* (CytoC) from the mitochondria, which, together with Apaf-1, cleaves and activates initiator and executioner caspases (Bratton and Salvesen, 2010). Surprisingly, we found that inhibition of MEK is sufficient to induce release of CytoC in all cell lines, and the release is enhanced by cotreatment with IFNβ (Figure 6B). We further confirmed that this behavior in single-cell fluorescent microscopy, which demonstrates that CytoC is released in all cells in both high- and low-pSTAT1 cell lines (Figures 6C and S5D). However, although MEK inhibition initiates the intrinsic pathway in high-pSTAT1 cell lines, and this response is enhanced by IFN, these cell lines fail to undergo apoptosis.

CytoC release leads to apoptosis by activating the caspase pathway. We found that caspase-9, an initiator caspase, and caspases-7 and -3, executioner caspases, are cleaved following the release of CytoC by MEK inhibition in low-pSTAT1 cell lines only (Figures 6D and S5E). Combinatorial treatment leads to a stronger and faster activation of these two caspases, but IFNβ treatment alone does not activate them (Figures 6D and S5E). Importantly, caspases are not cleaved in high-pSTAT1 cell lines, although CytoC is released. To confirm the association between pSTAT1 levels and caspase activation, we extended our panel to ten cell lines, adding two additional high- and two additional low-pSTAT1 cell lines. As with the original set of cell lines, caspases are cleaved only in low-pSTAT1 cell lines (Figure S5E). The lack of caspase activation may explain the cytotoxic resistance to treatment.
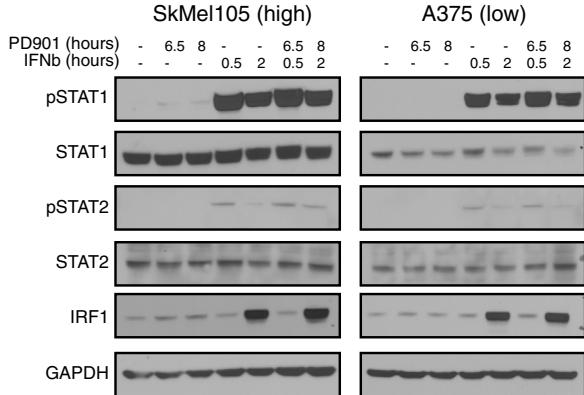
Additional components, such as APAF-1, cIAP1-2, and XIAP, play parts in the activation of the caspase pathway (Soengas et al., 2001). We therefore assessed the baseline expression levels of these proteins in our cell line panel, but found no correlation between their levels and the cytotoxic response to the treatments (Figures S5F and S5G). Additionally, we confirmed that caspase-9, the upstream caspase of the caspase pathway (Riedl and Shi, 2004), is expressed in comparable levels in all cell lines (Figure S5F).

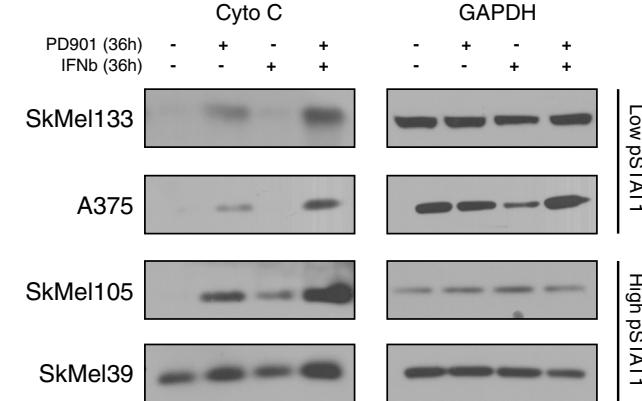### Deletion of Interferon Locus Correlates with Cytotoxic Response

Basal activity of the interferon pathway predicts the cytotoxic response to MEK inhibition and its combination with IFNα/β. Levels of pathway inhibitors from the SOCS and PIAS family are similar in all cell lines and fail to explain the differences in the basal activation of the pathway (Figure S6A). We therefore sought to identify genetic lesions that could be responsible for the differential basal activation of this pathway.

Using the large number of samples in The Cancer Genome Atlas (TCGA) melanoma data set, we associated STAT1 pathway activity levels with genetic aberrations (see Experimental Procedures). To infer pathway activity, we used the genes in the STAT1 cluster identified by COSPER. This gene cluster reflects pSTAT1 levels and is also highly correlated in the TCGA data set (Figure 7A).
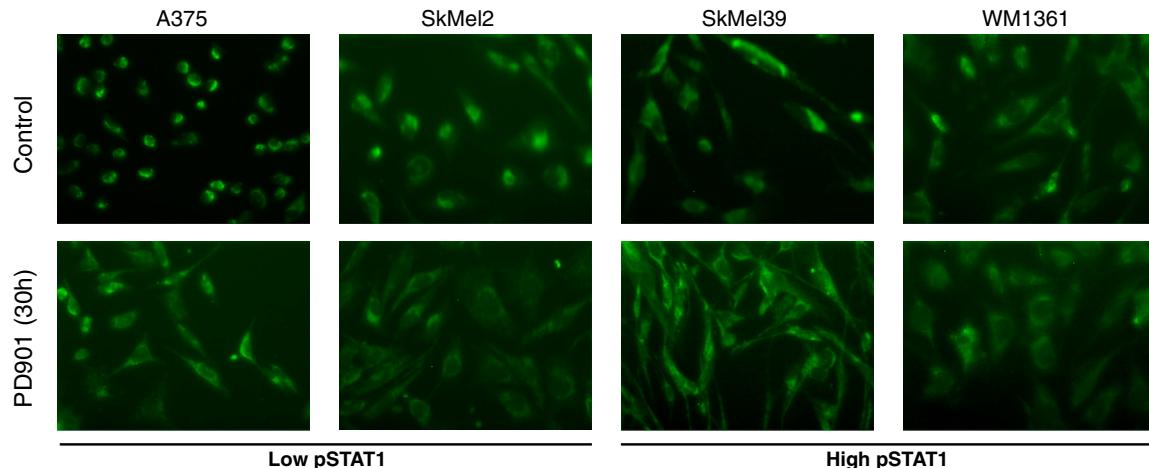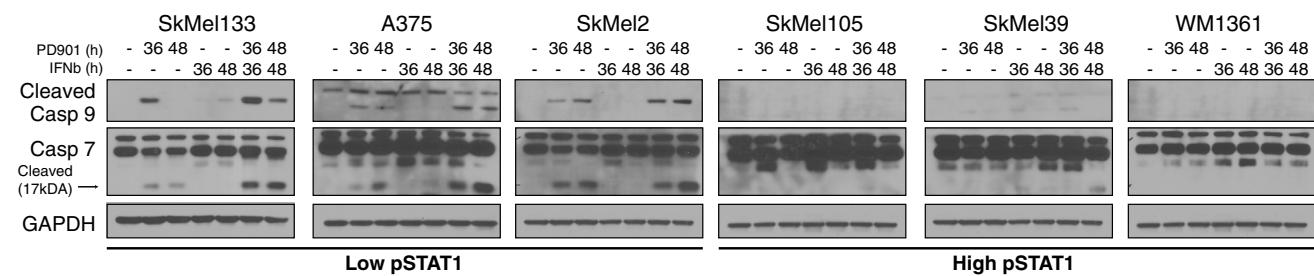
Figure 6. Elucidating the Cytotoxic Response of IFNβ and MEKi

(A) Response to IFNβ, as measured by pSTAT1 and IRF1 levels, is similar in both high- and low- pSTAT1 cell lines, and MEK inhibition doesn't alter the response (for transcriptional response, see Figure S5B). Notably, basal activity level of the pathway in high-pSTAT1 cell lines is much lower than the induction in pathway activity after IFNβ treatment.

(B) MEKi activates the intrinsic apoptotic pathway by CytoC release from the mitochondria, ~36 hr after treatment. IFNβ enhances the response in all cell lines, including the high-pSTAT1-resistant cell lines.

(C) Fluorescent microscopy staining of CytoC shows similar patterns of CytoC release in both high- and low-pSTAT1 cell lines. CytoC is released from the mitochondria in all cells following MEK inhibition. See Figure S5D for the images with nucleus staining.

(D) Caspase-7 and -9 are cleaved and activated following MEK inhibition in low-pSTAT1 cell lines only. IFNβ enhances this effect but fails to activate the pathway by itself. Both caspases are not cleaved in high-pSTAT1 cell lines. To reinforce the association between STAT1 levels and response to MEK inhibition, we tested four more cell lines. Both high- and low-pSTAT1 levels respond with accordance to their STAT1 levels (Figure S5E).
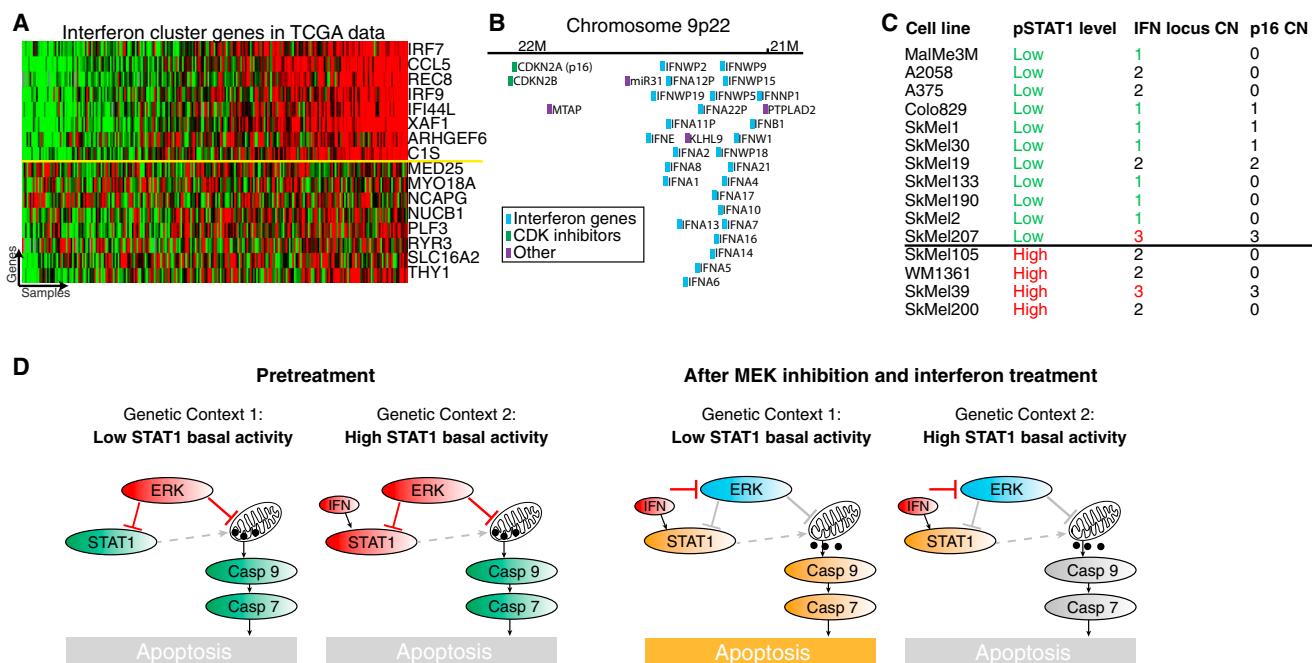
CellPress

Figure 7. Deletion of Interferon Locus and IFN Expression Levels Explains the Two Interferon-Pathway States and Predicts Drug Response

(A) The interferon gene cluster identified by COSPER is highly correlated in the TCGA melanoma expression data set. This allows us to infer pathway activity in the TCGA tumors and associate it with DNA aberrations. Genes above the yellow line were used for association with DNA copy number.

(B) The interferon locus contains 26 interferon genes and is only 0.5 Mb downstream of *CDKN2A* (*p16*), a known melanoma tumor suppressor.

(C) Interferon locus copy number is also correlated with pathway activity in our 14 cell line panel (p value = 0.05). *p16*, however, only 0.5 Mb upstream, is not, suggesting that interferon deletion and *p16* deletion are two independent events. SkMel200, a high-pSTAT1 cell line, was added for purposes of CNV analysis. Copy number of the interferon locus is also correlated with expression levels of interferon genes (Figure S6B), and conditioned media experiment shows that cytokines are released from high-pSTAT1 cell lines (Figure S6C).

(D) A cartoon depicting the two network states, before and after MEKi and IFN treatment. Inhibition of MEK leads to CytoC release in both cellular contexts, and IFN treatment enhances the response. However, caspase-9 is cleaved and activated only in low-pSTAT1 cell lines.

The copy number alteration most significantly associated with the STAT1 gene signature is a deletion of the interferon locus (q value = 10^{-4}, FDR; Storey and Tibshirani, 2003), located in chromosome 9p22. The locus contains a cluster of 26 interferon genes (Figure 7B), and deletion of this locus corresponds to low basal activity of the interferon pathway. Our panel confirms this association—most cell lines with low pathway activity have zero or one copy of the 9p22 locus, while all cell lines with high activity have two or three copies (Figure 7C, p value = 0.05; see Experimental Procedures for copy number assessment).

Interestingly, the interferon gene cluster on locus 9p22 is only 0.5 Mbs downstream of p16 (*CDKN2A*) (Figure 7B), a known tumor suppressor gene deleted in roughly 60% of melanoma tumors (Reed et al., 1995). Deletion of both *p16* and the interferon locus was previously reported (Naylor et al., 1997), but as research focused on the role p16 in cancer, deletion of the interferon locus was viewed as a passenger mutation. However, copy number data show that both events are independent, and copy number of the interferon locus and not *p16* is associated with the cytotoxic response to MEK inhibition (Figure 7C).

We confirmed that an autocrine loop is responsible for the lower levels of pSTAT1, using a conditioned media experiment. In these experiments media from high-pSTAT1 cell lines lead to activation of STAT1 in low-pSTAT1 cell lines (Figure S6C),

confirming that high-pSTAT1 cell lines that harbor two copies of the interferon locus produce and release cytokines, presumably IFN, which leads to STAT1 activation.

To summarize, our results show that cell lines with fewer copies of the interferon locus and lower expression of the interferon genes are sensitive to the cytotoxic effects of MEK inhibition (Figure 7D). Furthermore, IFNα/β enhances this cytotoxic response via an increase in CytoC release from the mitochondria. However, cell lines with high basal activity of the interferon pathway are resistant to the cytotoxic effects of the treatments, and although MEK inhibition leads to CytoC release in these cell lines, it seems that an impairment of the caspase activation mechanism leads to apoptosis aversion. Taken together, we postulate that constitutive exposure to IFN is adverse to cancer cells, and they overcome it by either deactivation of the interferon pathway or by an impairment of the apoptotic pathway.

DISCUSSION

Contemporary cancer drug development focuses on targeting recurring oncogenic events, such as gene amplification and overexpression (*HER2*) or activation (BRAF). This approach is based on the principle of oncogene addiction. The underlying

assumption is that the downstream targets of the oncogenes are the same in all tumors. Drug combinations are also suggested based on the principle of similar network structure and pathway dependencies in tumors harboring specific oncogenic mutations.

However, our analysis of MAPK targets in MAPK-activated melanomas reveals tremendous differences in underlying network structure between tumors. Although we analyzed the transcriptional output of MEK inhibition only in MAPK-activated melanoma cell lines, each cell line had a unique transcriptional response. Moreover, a vast majority of downstream targets of the MAPK pathway are *context-specific*—under the control of the pathway in only a subset of cell lines.

To detect context-specific targets using pre- and postinhibition expression data, we developed COSPER, a biclustering algorithm that identifies coexpressed genes that are under the control of the MAPK pathway in only a subset of cell lines. There are several benefits to identifying clusters of context-specific, coregulated genes. First, we can apply enrichment analysis to the coexpressed genes and identify the pathway that likely regulates their expression. Second, by using postinhibition data to narrow the gene set to only those that respond to perturbation, we specifically search for pathways regulated by the MAPK pathway. Third, the context—partitioning the cell lines into two groups—can assist in the identification of genetic aberrations that are more frequent in one group versus the other, thus also associating a genetic lesion with pathway activation. Fourth, the subgrouping of cell lines can also be associated with a phenotype, such as growth rate, response to treatment, "stem cell-ness," and others. Together, context-specific coregulated clusters link genetic lesions to a MAPK-regulated pathway and a phenotype, and can assist in the understanding of response heterogeneity.

Using COSPER, we identified a possible interaction between MEK inhibition and IFNα/β, two approved treatments for melanoma. An experimental validation uncovered two key findings: first, IFNα/β enhances the cytotoxic response of MEK inhibition; second, cell lines with high basal activity of the interferon pathway exhibit much lower cytotoxicity under MEK inhibition. We found that a deletion of the interferon locus is correlated with, and explains, the basal activity level of the interferon pathway, and therefore predicts the cytotoxic response to MEK inhibition. However, our results indicate that the basal activity level is not the mechanism for the sensitivity and resistance to IFNα/β and MEK inhibition. Instead, we found an impairment of the caspase activation mechanism that may explain the cytotoxic resistance.

Although MEK inhibition leads to, and IFNβ increases, the release of CytoC from the mitochondria in all cell lines, regardless of their interferon-pathway basal activity level, caspases 9, 7, and 3 are activated only in cell lines with low interferon pathway activity. We failed, however, to identify the lesion that prevents caspase activation in cell lines with high interferon pathway activity. Understanding the mechanism of resistance can support the development of new drugs and treatments.

Taken together, these results suggest that constitutive exposure to IFN is adverse to cancer cells, and they overcome it by either deactivation of the interferon pathway or an impairment

of the apoptotic pathway. Weichselbaum et al. have previously linked interferon to drug response (Weichselbaum et al., 2008), showing that interferon pathway activity predicts survival of breast cancer patients following chemotherapy and radiation. Our analysis of the TCGA data shows that a lower basal activity of the interferon pathway in breast cancer is associated with a deletion of IRF1, Interferon Response Factor 1, a necessary protein for interferon-induced death (data not shown) (Sancéau et al., 2000).

The interferon pathway might have important clinical implications in melanoma and other cancers. Since interferon pathway activity predicts the cytotoxic response to MEK inhibition in vitro, it is possible that its signaling activity, interferon expression levels, and/or interferon locus copy number can be used as a biomarker for treatment by MAPK pathway inhibitors. The clinical implications of IFNα/β treatment, however, are less straightforward, and further studies are necessary to check whether in the therapeutic window of IFN it has tumor-specific effect.

To summarize, our work demonstrates that tumor networks are more complex and varied than previously appreciated. Although only MAPK-activated melanoma cell lines were examined, these were found to be heterogeneous and immensely varied. Moreover, while all BRAF mutant tumors are grouped together and treated similarly in the clinic, the targets and pathways regulated by BRAF in different cell lines are vastly different. Even with a small sample size of only 14 cell lines, pre- and post-perturbation expression data empower the discovery of dependencies and interactions between pathways. We believe that a similar analysis of larger data sets of pre- and postinhibition expression data can help identify additional context-specific interactions.

Postperturbation data significantly enhance the ability to identify downstream targets (Niepel et al., 2013; Sachs et al., 2005). Perturbations break correlated patterns, resolve cause and effect, and reveal regulation patterns that are not observed in steady-state expression levels. It was previously shown that response to perturbation varies significantly, even in cancer subtypes that share similar oncogenic mutations (Duncan et al., 2012; Niepel et al., 2014). However, analysis of postperturbation protein levels typically focuses only on postperturbation changes. When an important pathway such as MAPK is inhibited, many of the differentially expressed genes involve response to stress, rather than genes that were regulated by the pathway prior to the perturbation. Typical methods would consider these MAPK targets (and indeed these respond to MAPK inhibition); however, these are not regulated by MAPK in physiological conditions, prior to MAPK inhibition. COSPER can distinguish these using expression patterns prior to perturbation. Moreover, COSPER takes *context* into account. This allows us to identify gene clusters that only change in subsets of cell lines, which would likely be dismissed by other methods. By comparing both pre- and postperturbation gene expression, and taking context into account, we can better identify pathways that are regulated by MAPK in each cancer cell line. Therefore, by combining information from both pre- and postperturbation levels, we reveal the network structure governed by MAPK and the differences in this structure in difference cell lines.

CellPress

The full scale of these differences is only revealed when examining a perturbed network, which highlights the importance of postinhibition data, compared with steady-state data only. We believe that our research has only scratched the surface, and future studies with larger cohort size should be conducted, as our data demonstrate the value of system-wide perturbation analysis of tumors in the era of personalized medicine.

EXPERIMENTAL PROCEDURES

Cell Culture and Drug Treatment

Cell lines were obtained from A. Houghton (Memorial Sloan-Kettering Cancer Center), except for Colo829 and A2058, which were purchased from ATCC. All cell lines were maintained in RPMI 1640 (Invitrogen 21870-092), supplemented with 2 mM glutamine, 50 units/mL penicillin, 50 units/mL streptomycin, and 10% FBS (Omega Scientific), and incubated at 37°C in 5% CO2.

Samples for protein and gene expression analysis were plated at 60%–80% confluency and incubated for 20–24 hr, then treated with PD325901 (50 nM), interferon alpha (20,000 U/mL, R&D 11100), or interferon beta (1,000 U/mL, R&D 11415). Control samples were collected untreated at time of treatment.

Gene Expression and Microarrays

Agilent's 8 × 60 human gene expression was used, and samples were harvested 8 hr posttreatment. Experimental procedures and data normalization are described in Supplemental Information.

We used Agilent's 1 M SurePrint CGH arrays to assess copy number. DNA was extracted using QIAGEN's DNeasy kit and labeled and hybridized according to Agilent's protocol.

TCGA Data Analysis

TCGA expression and CGH data were downloaded from the TCGA website. Genes for the STAT1 gene signature were a subset of COSPER's STAT1 signature. All genes with a Pearson $r^2 > 0.5$ with at least three additional genes were included. Association with copy number was performed using Pearson correlation between the mean of the gene signature and copy number levels of each gene. Pearson's p values were corrected by FDR (Storey and Tibshirani, 2003).

Protein Levels

Samples for protein analysis were lysed using RIPA buffer. Protein concentration was assessed using BCA staining. Samples were then normalized to a fixed concentration and mixed with a 5× glycerol/SDS/DTT loading buffer. Lysates were run on gradient (4%–12%) Bis-Tris gels. Primary antibodies are listed in Table S3. After incubation with horseradish peroxidase- conjugated secondary antibodies, proteins were detected using chemiluminescence.

CytoC release was assessed on fresh unfrozen pellets using sucrose/mannitol buffer (Majewski et al., 2004). Full details are in the Supplemental Information. Protocol for CytoC staining in fluorescent microscopy is detailed in Supplemental Information.

Growth Curves and Apoptosis Levels

For growth curve measurement, 50,000 cells were plated in 6-well plates with 2 mL of growth media. Cells were counted every 24 hr following treatment using a cell counter (Coulter Z1), in triplicates.

Apoptosis was assessed by TUNEL staining. Cells were plated in 6-well plates at 200,000 cells/well. Twenty-four hours after plating, cells were treated with PD325901, and both floating and adherent cells were collected 72 hr after treatment. TUNEL was performed using Invitrogen BrdU TUNEL kit.

Context-Specific Computational Model

A full description of COSPER can be found in the Supplemental Information. In short, all genes are scored for all possible splits using both pre- and posttreatment expression using the NormalGamma function. Genes with a strong association with a split join its cluster. Then similar clusters are merged, leaving fewer clusters with more genes each.

REFERENCES

Barretina, J., Caponigro, G., Stransky, N., Venkatesan, K., Margolin, A.A., Kim, S., Wilson, C.J., Lehár, J., Kryukov, G.V., Sonkin, D., et al. (2012). The Cancer Cell Line Encyclopedia enables predictive modelling of anticancer drug sensitivity. Nature 483, 603–607.

Bratton, S.B., and Salvesen, G.S. (2010). Regulation of the Apaf-1-caspase-9 apoptosome. J. Cell Sci. 123, 3209–3214.

Dai, B., Meng, J., Peyton, M., Girard, L., Bornmann, W.G., Ji, L., Minna, J.D., Fang, B., and Roth, J.A. (2011). STAT3 mediates resistance to MEK inhibitor through microRNA miR-17. Cancer Res. 71, 3658–3668.

Duncan, J.S., Whittle, M.C., Nakamura, K., Abell, A.N., Midland, A.A., Zawistowski, J.S., Johnson, N.L., Granger, D.A., Jordan, N.V., Darr, D.B., et al. (2012). Dynamic reprogramming of the kinome in response to targeted MEK inhibition in triple-negative breast cancer. Cell 149, 307–321.

Flaherty, K.T., Puzanov, I., Kim, K.B., Ribas, A., McArthur, G.A., Sosman, J.A., O'Dwyer, P.J., Lee, R.J., Grippo, J.F., Nolop, K., and Chapman, P.B. (2010). Inhibition of mutated, activated BRAF in metastatic melanoma. N. Engl. J. Med. 363, 809–819.

Garnett, M.J., Edelman, E.J., Heidorn, S.J., Greenman, C.D., Dastur, A., Lau, K.W., Greninger, P., Thompson, I.R., Luo, X., Soares, J., et al. (2012). Systematic identification of genomic markers of drug sensitivity in cancer cells. Nature 483, 570–575.

Hecker, M., Hartmann, C., Kandulski, O., Paap, B.K., Koczan, D., Thiesen, H.J., and Zettl, U.K. (2013). Interferon-beta therapy in multiple sclerosis: the short-term and long-term effects on the patients' individual gene expression in peripheral blood. Mol. Neurobiol. 48, 737–756.

Hodis, E., Watson, I.R., Kryukov, G.V., Arold, S.T., Imielinski, M., Theurillat, J.P., Nickerson, E., Auclair, D., Li, L., Place, C., et al. (2012). A landscape of driver mutations in melanoma. Cell 150, 251–263.

Jackson, D.P., Watling, D., Rogers, N.C., Banks, R.E., Kerr, I.M., Selby, P.J., and Patel, P.M. (2003). The JAK/STAT pathway is not sufficient to sustain the antiproliferative response in an interferon-resistant human melanoma cell line. Melanoma Res. 13, 219–229.

Johannessen, C.M., Johnson, L.A., Piccioni, F., Townes, A., Frederick, D.T., Donahue, M.K., Narayan, R., Flaherty, K.T., Wargo, J.A., Root, D.E., and Garraway, L.A. (2013). A melanocyte lineage program confers resistance to MAP kinase pathway inhibition. Nature 504, 138–142.

Joseph, E.W., Pratilas, C.A., Poulikakos, P.I., Tadi, M., Wang, W., Taylor, B.S., Halilovic, E., Persaud, Y., Xing, F., Viale, A., et al. (2010). The RAF inhibitor PLX4032 inhibits ERK signaling and tumor cell proliferation in a V600E BRAF-selective manner. Proc. Natl. Acad. Sci. USA *107*, 14903–14908.

Leaman, D.W., Chawla-Sarkar, M., Jacobs, B., Vyas, K., Sun, Y., Ozdemir, A., Yi, T., Williams, B.R., and Borden, E.C. (2003). Novel growth and death related interferon-stimulated genes (ISGs) in melanoma: greater potency of IFN-beta compared with IFN-alpha2. J. Interferon Cytokine Res. *23*, 745–756.

Levy, C., Khaled, M., and Fisher, D.E. (2006). MITF: master regulator of melanocyte development and melanoma oncogene. Trends Mol. Med. *12*, 406–414.

Lito, P., Pratilas, C.A., Joseph, E.W., Tadi, M., Halilovic, E., Zubrowski, M., Huang, A., Wong, W.L., Callahan, M.K., Merghoub, T., et al. (2012). Relief of profound feedback inhibition of mitogenic signaling by RAF inhibitors attenuates their activity in BRAFV600E melanomas. Cancer Cell *22*, 668–682.

Majewski, N., Nogueira, V., Bhaskar, P., Coy, P.E., Skeen, J.E., Gottlob, K., Chandel, N.S., Thompson, C.B., Robey, R.B., and Hay, N. (2004). Hexokinase-mitochondria interaction mediated by Akt is required to inhibit apoptosis in the presence or absence of Bax and Bak. Mol. Cell *16*, 819–830.

Naylor, M.F., Brown, S., Quinlan, C., Pitha, J.V., and Evertt, M.A. (1997). 9p21 deletions in primary melanoma. Dermatol. Online J. *3*, 1.

Niepel, M., Hafner, M., Pace, E.A., Chung, M., Chai, D.H., Zhou, L., Schoeberl, B., and Sorger, P.K. (2013). Profiles of Basal and stimulated receptor signaling networks predict drug response in breast cancer lines. Sci. Signal. *6*, ra84.

Niepel, M., Hafner, M., Pace, E.A., Chung, M., Chai, D.H., Zhou, L., Muhlich, J.L., Schoeberl, B., and Sorger, P.K. (2014). Analysis of growth factor signaling in genetically diverse breast cancer lines. BMC Biol. *12*, 20.

Paraiso, K.H., Xiang, Y., Rebecca, V.W., Abel, E.V., Chen, Y.A., Munko, A.C., Wood, E., Fedorenko, I.V., Sondak, V.K., Anderson, A.R., et al. (2011). PTEN loss confers BRAF inhibitor resistance to melanoma cells through the suppression of BIM expression. Cancer Res. *71*, 2750–2760.

Platanias, L.C. (2005). Mechanisms of type-I- and type-II-interferon-mediated signalling. Nat. Rev. Immunol. *5*, 375–386.

Poulikakos, P.I., Zhang, C., Bollag, G., Shokat, K.M., and Rosen, N. (2010). RAF inhibitors transactivate RAF dimers and ERK signalling in cells with wild-type BRAF. Nature *464*, 427–430.

Pratilas, C.A., Taylor, B.S., Ye, Q., Viale, A., Sander, C., Solit, D.B., and Rosen, N. (2009). (V600E)BRAF is associated with disabled feedback inhibition of RAF-MEK signaling and elevated transcriptional output of the pathway. Proc. Natl. Acad. Sci. USA *106*, 4519–4524.

Reed, J.A., Loganzo, F., Jr., Shea, C.R., Walker, G.J., Flores, J.F., Glendening, J.M., Bogdany, J.K., Shiel, M.J., Haluska, F.G., Fountain, J.W., et al. (1995). Loss of expression of the p16/cyclin-dependent kinase inhibitor 2 tumor suppressor gene in melanocytic lesions correlates with invasive stage of tumor progression. Cancer Res. *55*, 2713–2718.

Riedl, S.J., and Shi, Y. (2004). Molecular mechanisms of caspase regulation during apoptosis. Nat. Rev. Mol. Cell Biol. *5*, 897–907.

Sachs, K., Perez, O., Pe'er, D., Lauffenburger, D.A., and Nolan, G.P. (2005). Causal protein-signaling networks derived from multiparameter single-cell data. Science *308*, 523–529.

Sancéau, J., Hiscott, J., Delattre, O., and Wietzerbin, J. (2000). IFN-beta induces serine phosphorylation of Stat-1 in Ewing's sarcoma cells and mediates apoptosis via induction of IRF-1 and activation of caspase-7. Oncogene *19*, 3372–3383.

Slamon, D.J., Leyland-Jones, B., Shak, S., Fuchs, H., Paton, V., Bajamonde, A., Fleming, T., Eiermann, W., Wolter, J., Pegram, M., et al. (2001). Use of chemotherapy plus a monoclonal antibody against HER2 for metastatic breast cancer that overexpresses HER2. N. Engl. J. Med. *344*, 783–792.

Soengas, M.S., Capodieci, P., Polsky, D., Mora, J., Esteller, M., Opitz-Araya, X., McCombie, R., Herman, J.G., Gerald, W.L., Lazebnik, Y.A., et al. (2001). Inactivation of the apoptosis effector Apaf-1 in malignant melanoma. Nature *409*, 207–211.

Solit, D.B., Garraway, L.A., Pratilas, C.A., Sawai, A., Getz, G., Basso, A., Ye, Q., Lobo, J.M., She, Y., Osman, I., et al. (2006). BRAF mutation predicts sensitivity to MEK inhibition. Nature *439*, 358–362.

Sosman, J.A., Kim, K.B., Schuchter, L., Gonzalez, R., Pavlick, A.C., Weber, J.S., McArthur, G.A., Hutson, T.E., Moschos, S.J., Flaherty, K.T., et al. (2012). Survival in BRAF V600-mutant advanced melanoma treated with vemurafenib. N. Engl. J. Med. *366*, 707–714.

Storey, J.D., and Tibshirani, R. (2003). Statistical significance for genomewide studies. Proc. Natl. Acad. Sci. USA *100*, 9440–9445.

Tsai, J., Lee, J.T., Wang, W., Zhang, J., Cho, H., Mamo, S., Bremer, R., Gillette, S., Kong, J., Haass, N.K., et al. (2008). Discovery of a selective inhibitor of oncogenic B-Raf kinase with potent antimelanoma activity. Proc. Natl. Acad. Sci. USA *105*, 3041–3046.

Weichselbaum, R.R., Ishwaran, H., Yoon, T., Nuyten, D.S., Baker, S.W., Khodarev, N., Su, A.W., Shaikh, A.Y., Roach, P., Kreike, B., et al. (2008). An interferon-related gene signature for DNA damage resistance is a predictive marker for chemotherapy and radiation for breast cancer. Proc. Natl. Acad. Sci. USA *105*, 18490–18495.

Xing, F., Persaud, Y., Pratilas, C.A., Taylor, B.S., Janakiraman, M., She, Q.B., Gallardo, H., Liu, C., Merghoub, T., Hefter, B., et al. (2012). Concurrent loss of the PTEN and RB1 tumor suppressors attenuates RAF dependence in melanomas harboring (V600E)BRAF. Oncogene *31*, 446–457.

Zhang, J., Xiao, Z., Lai, D., Sun, J., He, C., Chu, Z., Ye, H., Chen, S., and Wang, J. (2012). miR-21, miR-17 and miR-19a induced by phosphatase of regenerating liver-3 promote the proliferation and metastasis of colon cancer. Br. J. Cancer *107*, 352–359.

Supplemental Information

Interferon α/β Enhances the Cytotoxic

Response of MEK Inhibition in Melanoma

Oren Litvin, Sarit Schwartz, Zhenmao Wan, Tanya Schild, Mark Rocco,
Nul Loren Oh, Bo-Juen Chen, Noel Goddard, Christine Pratilas, and Dana Pe'er

Supplementary figures

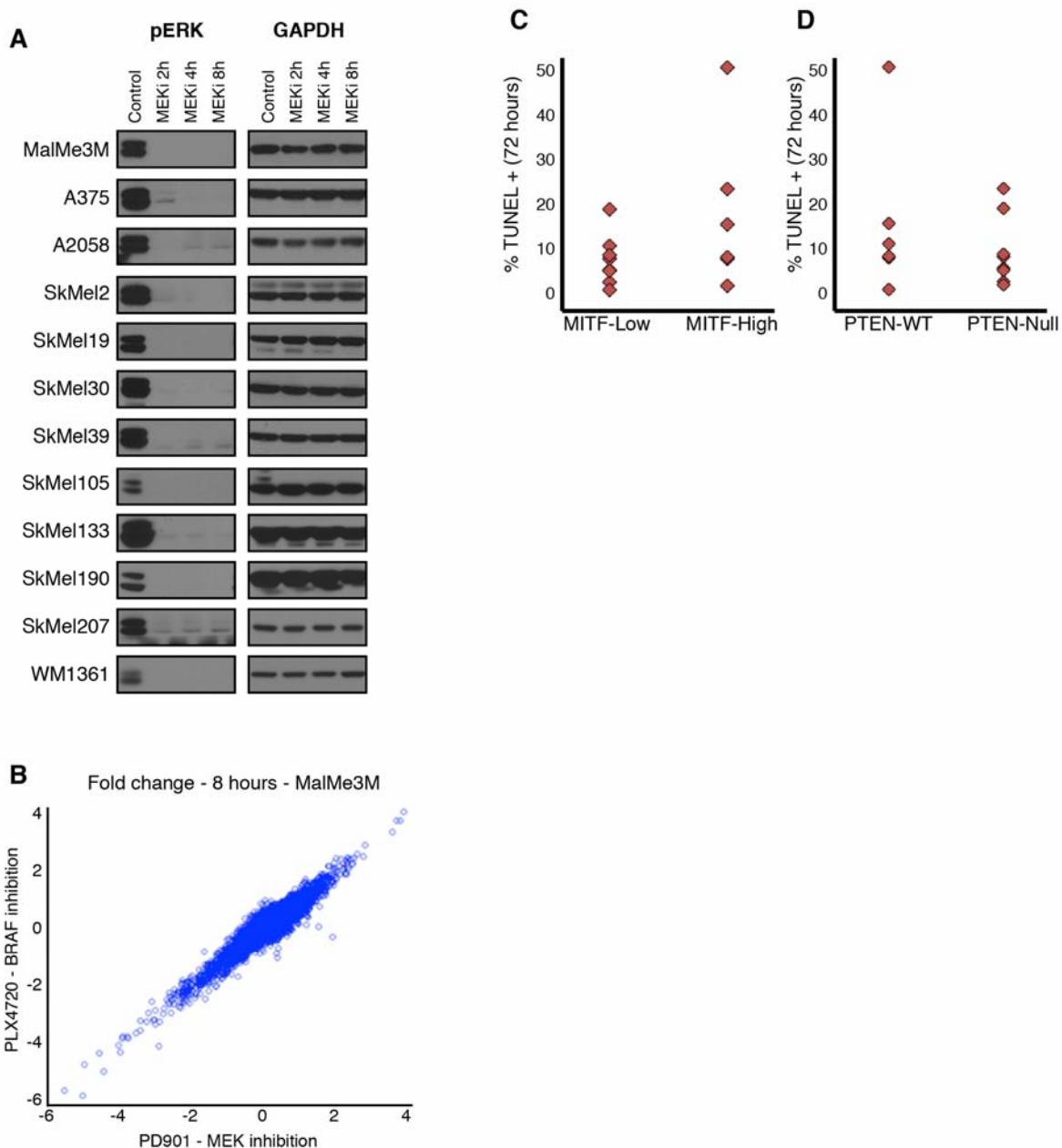**Figure S1** – Related to Figure 1 – Response to MAPK inhibition **A.** pERK levels in all cell lines, 2, 4 and 8 hours following treatment with PD901. pERK stays low throughput the 8 hours and therefore does not explain the heterogeneity observed between cell lines. **B.** Comparison of MEK and BRAF inhibitors in a BRAF-V600E cell line shows an almost identical transcriptional response. Scatter plot shows fold change of all genes

with a 50nM of PD325901, a MEK inhibitor (x-axis), compared with a 2uM of PLX4720, a BRAF inhibitor (y-axis). Almost all genes fall directly on the diagonal. Colo829 doesn't grow in the conditions used to generate these growth curves. **C-D**. Scatter plots representation of the data in figure 1B. Each dot represents the difference of percentage of TUNEL+ cells between PD901 and DMSO, dividing *MITF*+ and *MITF*- cell lines (B), and *PTEN*-WT and *PTEN*-null (C). These mutations do not fully explain the phenotypic differences between cell lines.
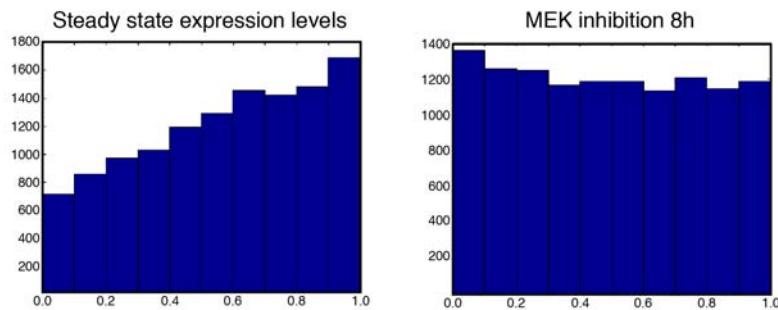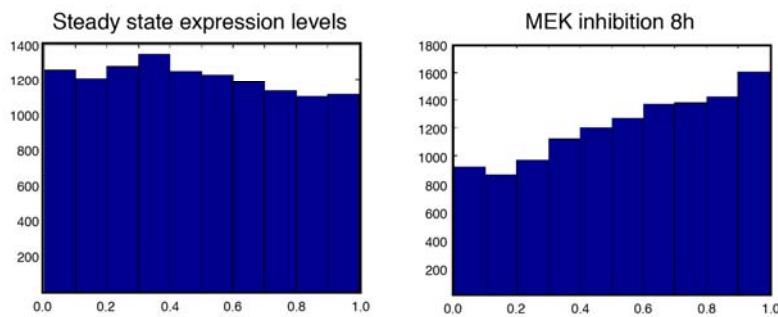
A t-test pvalues - BRAF mut vs. NRAS mut

Steady state expression levels   MEK inhibition 8h

B t-test pvalues - PTEN null vs. PTEN WT

Steady state expression levels   MEK inhibition 8h

Figure S2 – Related to figure 2 – Correlation between known genetic variants and gene expression - **A.** Histograms of p-values comparing expression levels of BRAF-mut with NRAS-mut cell lines using t-test, before and after pathway inhibition. No gene passes FDR correction with q-value<0.05. See number of targeted genes in figure 2. **B.** Histograms of p-values comparing expression levels of *PTEN*-null/mut with *PTEN*-WT in BRAF-mut cell lines using t-test, before and after pathway inhibition. No gene passes FDR correction with qvalue<0.05.
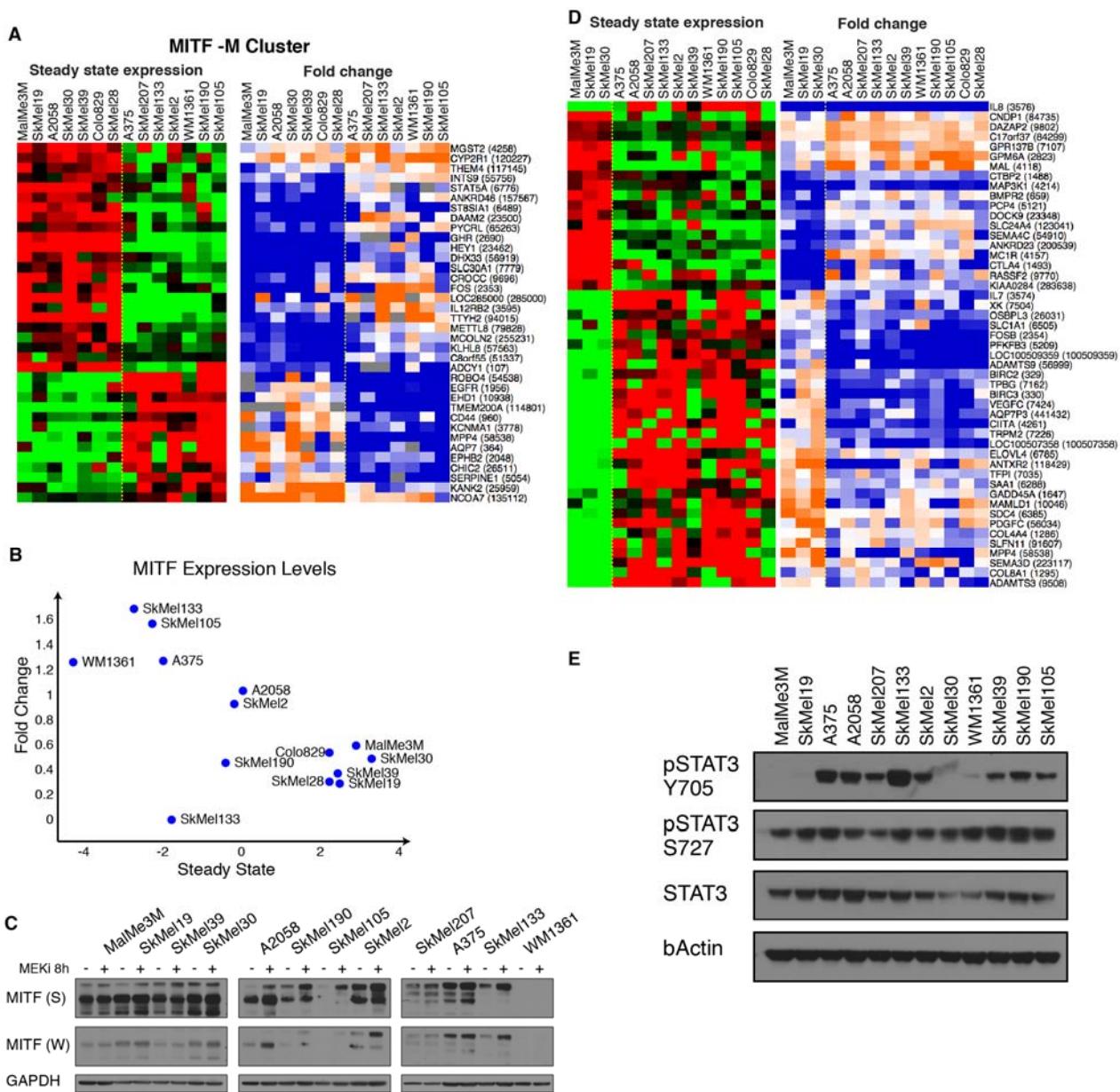
Figure S3 – Related to figure 4 – COSPER links pathway activity with gene expression levels - **A.** Full cluster, including all genes, of the cluster presented in figure 3A. **B.** *MITF* mRNA expression levels before (x-axis) and after (y-axis) MEK inhibition. Steady state and fold change levels are negatively correlated. **C.** Levels of MITF protein isoforms in 12 cell lines, before and 8 hours after MEK inhibition. Each isoform is regulated to different degrees in the different cell lines, supporting a context-specific control of MITF by the MAPK pathway.. Strong (S) and Weak (W) film exposures are shown. **D.** COSPER clusters together genes with the same context-specific regulation but with different regulation patterns. For example, the cluster here is associated with the STAT3

context, but contains 3 regulation patterns. The cluster in figure 4C shows one such pattern out of the 3 identified by COSPER. **E.** Levels of STAT3 and pSTAT3-S727 are similar in all cell lines and do not explain the differential activation of pSTAT3-Y705.
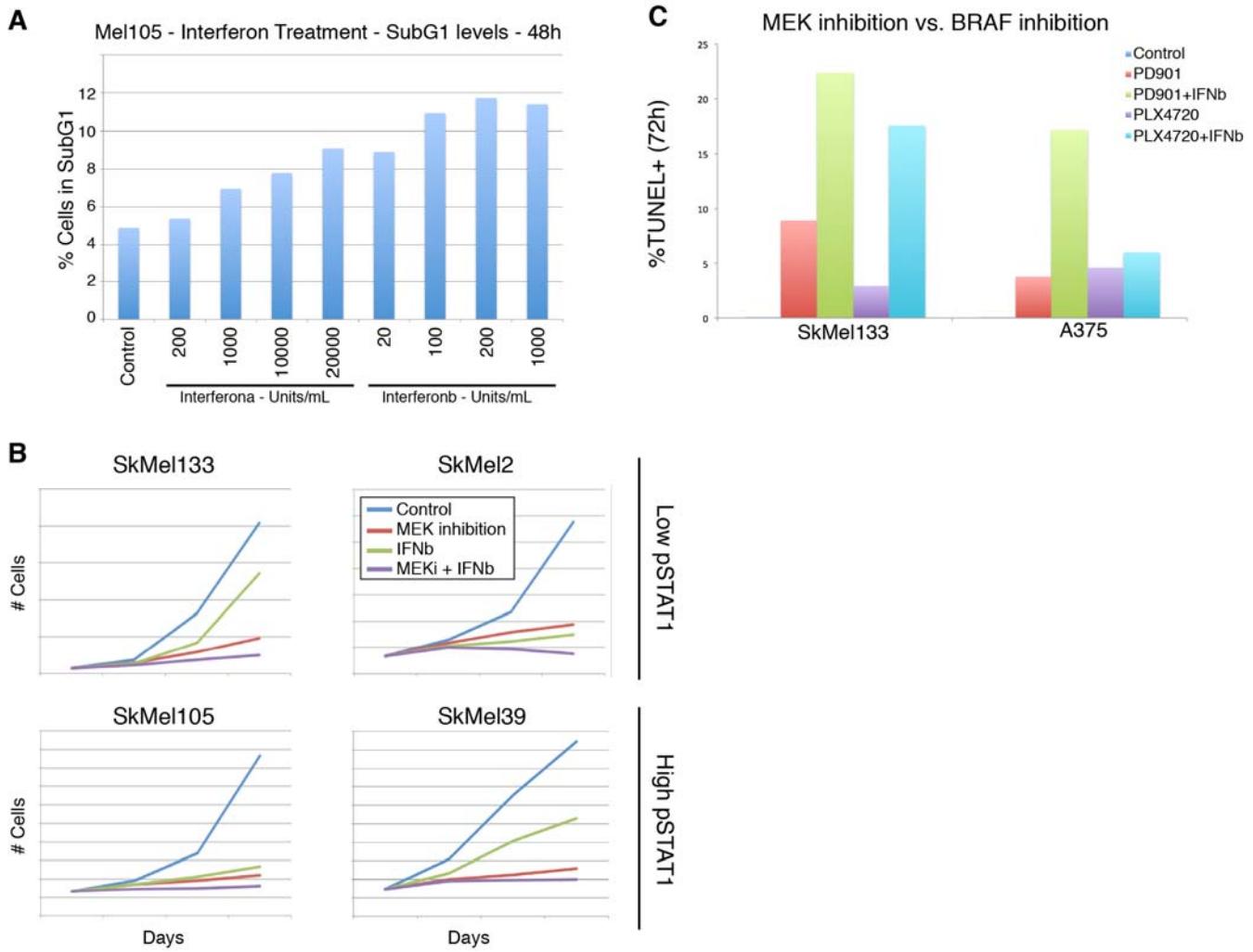
Figure S4 – Related to figure 5 – Response to IFNα/β treatment - **A.** Dose-dependent response to IFNα and β. The cytotoxicity of IFN was assessed in high pSTAT1 cell line, 48 hours after treatment using SubG1 percentage. IFNα has a weaker cytotoxic effect than IFNβ, and both show dose-dependent effects. 1000Units/mL of IFNβ was used for all experiments in this manuscript. Cells plated in 6 well plates, 200K cells/well, in 2mL of growth media. **B.** Growth curves of 2 low- (top) and 2 high- (bottom) pSTAT1 cell lines with MEK inhibition, IFNβ or both. 50K cells per well were plated in 6-well plates with 2mL of media and treated 24 hours later. Cells were counted every 24 hours up to 72 hours. Cytotoxic levels in figure 5E. **C.** Comparison of MEK inhibition and BRAF inhibition, with and without combination with IFNβ. Cells were plated in 6 well plates, 200K cells/well with 2mL media. 24 hours after plating cells were treated with DMSO, 50nM PD901 with or without IFNβ, 2uL of PLX4720 with or without IFNβ.

Figure S5 – Related to figure 6 – Identifying the mechanisms underlying response to treatment - **A.** Time course protein levels following treatment with IFNβ of one high

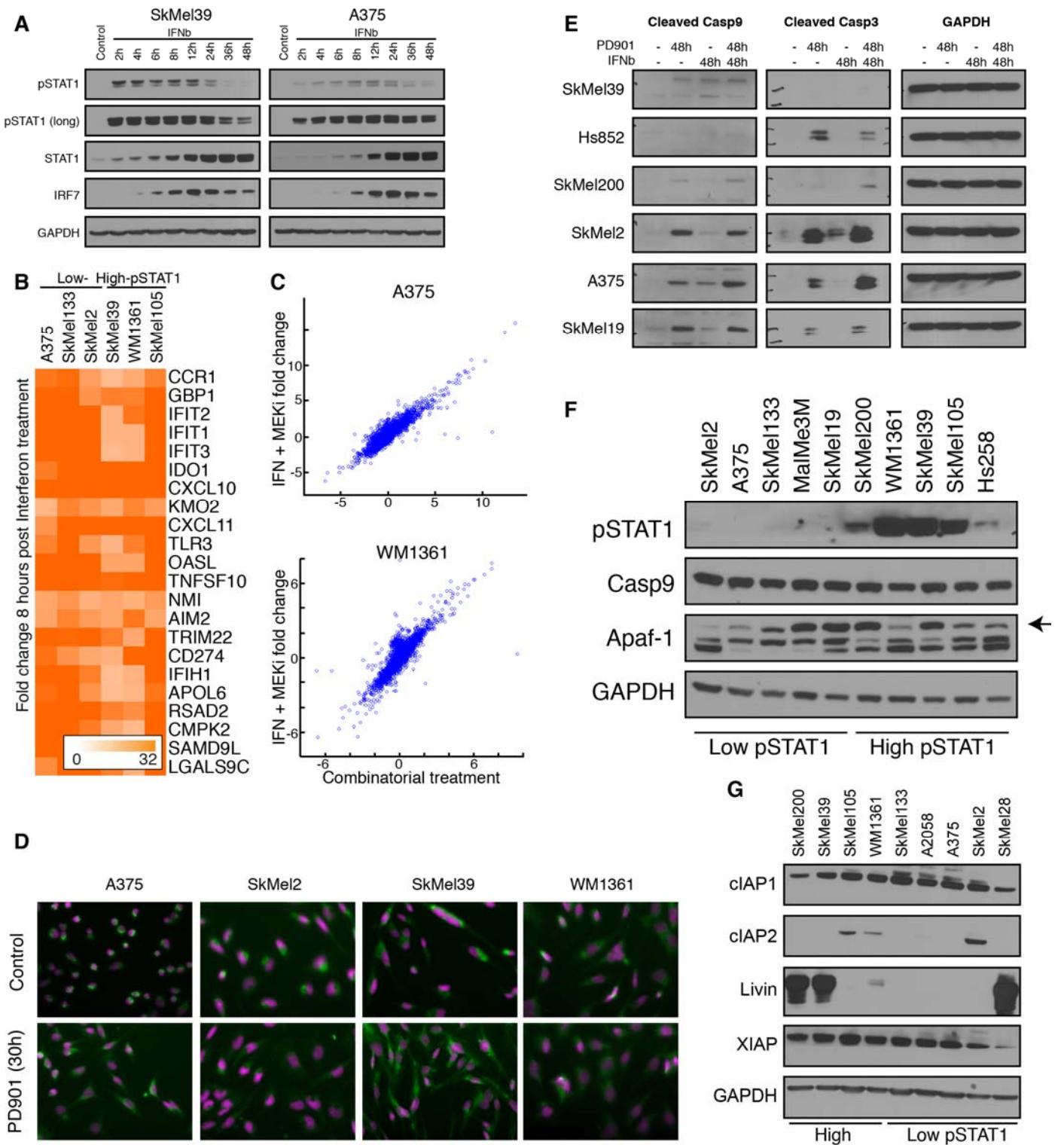pSTAT1 cell line (SkMel39) and one low (A375). Response amplitude and dynamics is almost identical in the two cell lines. **B.** 22 genes with the highest fold change following IFNβ treatment. The transcriptional response is similar in all cell lines, both with low- and high- basal activation of the pathway. Notably, the fold change of several genes reaches 100 fold, just 8 hours after treatment. **C.** Lack of synergistic and additive effects of MEK inhibition and IFNβ. Scatter plots show the fold change of all genes with a combination of MEK inhibition and IFN (x-axis) and the sum of fold changes with each treatment alone. Significant deviations from the diagonal represent synergism between drugs. Only one gene, *CCL4*, deviates from the diagonal in all 6 cell lines. **D.** Same as figure 6C, with DAPI staining to confirm nucleus positioning. **E.** Cleaved caspases 9 and 3 following MEK inhibition, IFN treatment, or their combination. This figure includes 4 cell lines that were not part of the original caspase analysis, and were included here to support the association between pSTAT1 levels and activation of the caspase pathway. **F.** Caspase 9 and APAF1 levels (arrow marks APAF1 band) are not correlated with pSTAT1 levels or with cytotoxic response to MEK inhibition. **G.** Levels of known caspase inhibitors are not correlated with the cytotoxic phenotype or pSTAT1 levels.
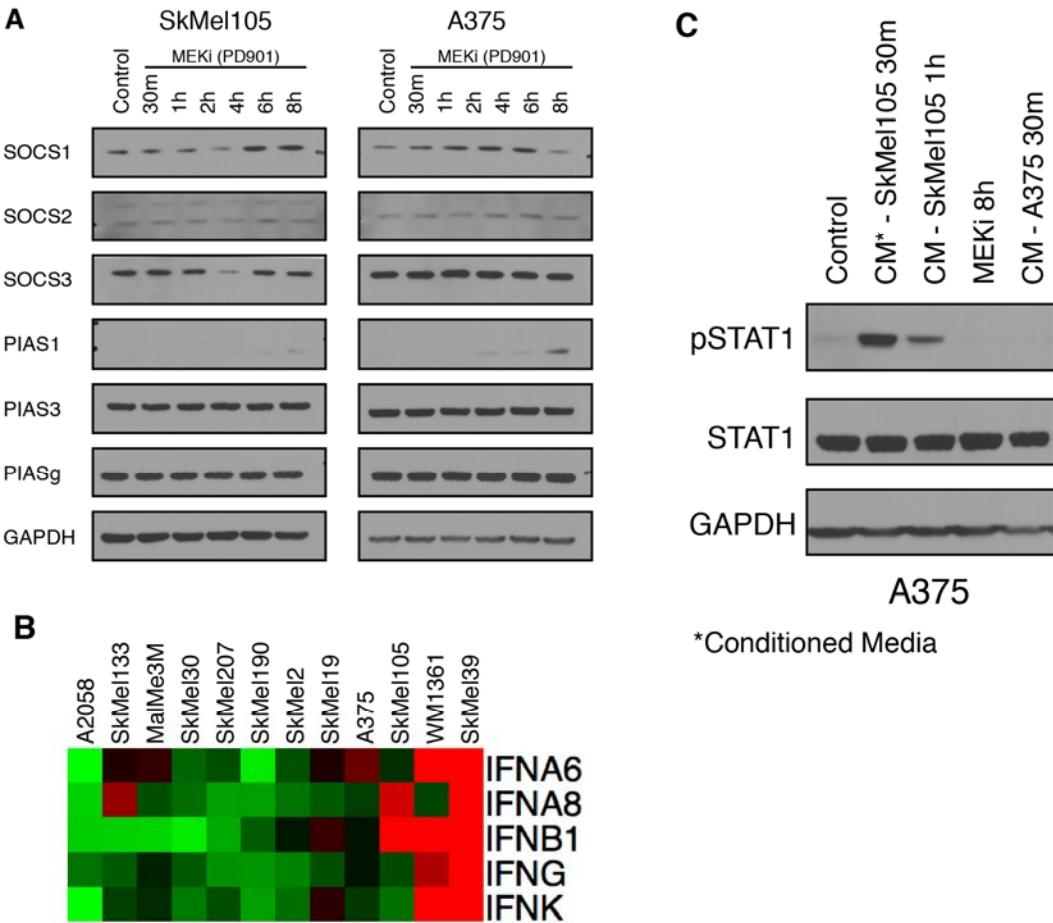
Figure S6 – Related to figure 7 – IFN levels regulated by an autocrine loop and deletion of IFN locus - **A.** Protein levels following MEK inhibition of 6 known inhibitors of the JAK-STAT pathway in two cell lines (SkMel105 - high pSTAT1, A375 – low pSTAT1). Most proteins don't change, although pSTAT1 goes up prior to 8h. Change of PIAS1 is similar in both cell lines. **B.** IFN genes with a significant differential expression between low- and high- pSTAT1 cell lines. *IFNA6*, *IFNA8* and *IFNB1* are located in the interferon locus (see figure 7). **C.** Conditioned media experiment shows that SkMel105, a high-pSTAT1 cell line, releases cytokines to the media that lead to the upregulation of pSTAT1. In this experiment, SkMel105 was cultured for 24h, and then the media was transferred to A375, a low-pSTAT1 cell line. Cells were collected 30m and 1h following media transfer. Lanes for MEK inhibition 8h and self-conditioned media (CM-A375) are shown as controls.

Supplementary tables

CTBP2	LDLRAP1
C14orf104	GSK3B
SLC20A2	HERC1
ZNF275	C5orf22
ADSS	TTC15
C8orf55	CREBL2
WDR75	DNAJC3
TRIM65	UBAC1
BAG5	SETD4
SSBP4	BTBD10
LYSMD2	CHD2
TMEM206	ANKRD54
SRXN1	GOT1
ZFAND1	IL16
RCC1	PPM1A
WDR74	CBFA2T2
JMJD4	C19orf12
MTHFD2	KDM4A
WDR89	RCBTB1
NOB1	HOMER3
ANKRD37	SNX30
ZBTB42	WDHD1
ACTR3B	FEM1B
PSMG4	MTMR10
LENG9	AKAP11
NR6A1	
BCORL1	
PAX3	
ABTB1	
ABR	
FNBP1L	
CNPPD1	
ZZZ3	
GNA13	
PEAK1	

Table S1 – List of genes from figure 2A

Gene symbols of the genes from figure 2A. The correlation of these genes with MITF levels is reveled only upon MEK inhibition.

Table S2 – In a separate excel file – List of COSPER modules (Materials and Methods)

Table S2 lists all modules identified by COSPER. Number of genes, and cell lines assigned to each of the contexts are listed for each module.

Antibody	Company	Catalog number
APAF-1	Abcam	Ab32372
Casp 7 (cleaved)	cell signaling	9492
Casp 9 (cleaved)	cell signaling	7237
Caspase 7	cell signaling	9492
Caspase 9	cell signaling	9508
cIAP1	cell signaling	7065
cIAP2	cell signaling	3130
Cytochrome C	abcam	ab110325
GAPDH	cell signaling	5174
IRF1	cell signaling	8478
IRF7	cell signaling	4920
Livin	cell signaling	5471
MITF	abcam	ab12039
pERK1/2	cell signaling	9101
PIAS1	cell signaling	3550
PIAS3	cell signaling	9042
PIASy	cell signaling	4392
pSTAT1 Y701	cell signaling	9167
pSTAT2	cell signaling	4441
pSTAT3 Y705	cell signaling	9138
SOCS1	cell signaling	3950
SOCS2	cell signaling	2779
SOCS3	cell signaling	2932
STAT1	cell signaling	9175
STAT2	cell signaling	4594
STAT3	cell signaling	9139
XIAP	cell signaling	2045

Table S3 – Related to Materials and Methods

List of antibodies used in this study.

Supplementary information

Microarray preprocessing

Samples for microarrays were harvested 8h post treatment. RNA was extracted using a Qiagen RNeasy kit, and labeled using Agilent's one-color labeling protocol. Labeled cRNA was hybridized to Agilent's 8x60 human gene expression arrays (expect for Colo829 and SkMel28 that were added to the panel after the first batch). MEK inhibition and basal state expression levels were measured in biological duplicates. Data normalization is described in supplementary material. Genatomy was used for data visualization and enrichment analysis (Litvin et al., 2009).

Agilent's software was used to assess raw signal intensity. Preprocessing of both the MEKi panel and the IFN experiment was similar. Each of the 3 batches were processed independently - MEKi panel 1, MEKi panel 2 and the IFN panel.

Preprocessing consists of 3 steps – probe filtering, data normalization and probe averaging.

Probe filtering

Log2 values were used from this point on. Probes were filtered based on their values. Probes with low or high levels in more than 20% of samples were removed. This was done to remove noisy and saturated probes. The lower and upper thresholds were different in different batches, depending on labeling, hybridization and scan levels:

Batch	Lower threshold	Upper threshold
MEKi panel 1	6	16
MEKi panel 2	7	18
IFN panel	7	17.5

Additionally, the Agilent probe flags were used to filter probes by a similar method: probes flagged in more than 20% of samples were removed. Flags that were used: will_above_bg, is_saturated, is_feat_non_uniform, is_feat_popn.

A "rescue" step was used to return probes representing genes that no probe was left to represent them. Probes representing the same gene with a high correlation (Pearson >0.75) were rescued. Additionally, probes with high SD (>3) were also rescued.

<u>Data normalization</u>

The 75th percentile of all samples was set to the average 75% by multiplying the values by a constant.

<u>Probe averaging</u>

Probes that measure the level of the same gene were averaged or filtered out.

If the average Pearson correlation between all probes is > .75, probes are averaged. If it is lower, the probe with the lowest correlation is removed. Process repeats till probes are averaged or only two probes are left. If only two probes left and the correlation is low, the probe with the higher raw intensity is chosen.

<u>Merging duplicates</u>

Baseline expression levels are mean-normalized at the gene level. Fold change is calculated against the control (baseline expression) of the cell line. Data from the two MEKi panels are combined at this point by averaging the baseline expression and fold change data.

COSPER - Context-Specific Regulation

COSPER – COntext SPEcific Regulation – is designed to identify genes that are directly regulated by the MAPK pathway (or any other perturbed pathway) in only a subset of cell lines. It is based on the assumption that genes under the direct control of a pathway are correlated before pathway inhibition and show a correlated expression change after pathway inhibition. Since we are looking for genes under the control of the pathway in only a subset of cell lines, we expect expression changes in only these cell lines.

COSPER uses pre-perturbation data to limit the search for genes under direct regulation of the perturbed pathway. After inhibition of a key signaling pathway such as MAPK, cellular events, such as metabolism, cell cycle and apoptosis, lead to expression changes of thousands of genes. Although the expression of those genes changes after MAPK inhibition, they are not *directly* regulated by MAPK. However, genes under the

direct control of MAPK pathway depend on its activation levels both before and after inhibition of the pathway. For example, *HEY1* (figure 3A) is under the control of MAPK in only a subset of cell lines. In *HEY1* case, it is overexpressed by MAPK in cell lines with high *MITF* levels. Therefore, only in *MITF*-high cell lines, *HEY1* expression levels decrease after MEK inhibition. Both pre- and post-inhibition expression levels are needed in order to determine this relationship.

COSPER is therefore designed to find genes with context-specific regulation patterns (figure 3B). It is consists of 3 major steps:

1. Gene level – identify binary splits with high scores for both baseline expression and fold change and construct clusters.
2. Merge related clusters – allows removal of spurious correlations and averaging the noise caused due to the small sample size.
3. Add high scoring genes to the remaining clusters

A detailed description of each of the steps follows the section on the NormalGamma score.

NormalGamma score

The algorithm is based on the NormalGamma score (DeGroot, 2004; Segal et al., 2003). The NormalGamma is a Bayesian score that takes variance, mean and number of data points into account. It gives a higher score to a data matrix with low variance.

We use this score since we are looking to reduce the variance of the samples. Our algorithm searches for genes that behave similarly in a subset of samples. For example, we are looking for a subset of samples where a predefined set of genes is up-regulated, compared with the rest of the samples where the genes are not under pathway control. Mathematically, this problem can be viewed as a subset of samples where the data have a lower variance compared with the variance of all samples combined. The NormalGamma score is driven mainly by data variance and is thus suitable for our needs.

The score:

$$N = size(data)$$

$$\beta = \max\left(1, \frac{\lambda(\alpha-2)}{\lambda+1}\right)$$

$$\beta_{plus} = \beta + \frac{Var(data)N}{2} + \frac{N\lambda|data|^2}{2(N+\lambda)}$$

$$\alpha_{plus} = \alpha + \frac{N}{2}$$

$$NormalGamma(data, \lambda, \alpha) = -N * \ln\left(\sqrt{2\pi}\right) + \frac{\ln\left(\frac{\lambda}{\lambda+N}\right)}{2} + \ln\left(\Gamma(\alpha_{plus})\right) - \ln\left(\Gamma(\alpha)\right) +$$

$$\alpha\ln(\beta) - \alpha_{plus}\ln(\beta_{plus})$$

The score used to assess the quality of the split is:

NormalGamma(right samples) + *NormalGamma*(left samples) - *NormalGamma*(all samples)

Step 1: Creating clusters

First, genes with low fold change and/or low variance in steady state are removed. Genes were considered only if they changed by more than 0.7 fold change (log2 scale) in at least 1 cell line, and at a steady-state expression value of 0.4 in at least 2 samples (to remove genes with extreme outliers in one sample that pass a standard-deviation based threshold). Additionally, all long non-coding RNA transcripts were removed. 5391 genes remain for further analysis.

Then, gene expression is normalized. Basal expression levels of each gene are set to have μ=0 and σ =1. Fold change for each gene is standardized only (σ =1).

Next, clusters are built bottom-up – genes are assigned to "splits", and a split with more than one gene assigned to it is considered a cluster. However, in order to filter out spurious associations we only consider clusters with 5 or more genes. All genes are tested across all valid binary splits. A valid split assigns at least 2 samples to each sample group. The test is based on permutations and the NormalGamma score.

A gene is assigned to a split if its NormalGamma scores (as defined in the previous section) in both the baseline expression and fold change are better than 99% of the split

permutations (pvalue<0.01). Additionally, in order to keep the best split-gene pairs only, an additional threshold is used:

NormalGamma (right)+ *NormalGamma* (left)- *NormalGamma*(all samples)>1

To determine whether clusters with more than 5 genes can be constructed by chance. We permuted the samples in the fold change expression data and performed this step on the permutated data. No clusters with 5 or more genes were constructed. Hence we believe the resulting clusters represent biological phenomenon.

Step 2: Merging clusters

A gene assigned to a split is very likely to be assigned to similar splits. A similar split might have one or more samples switching "sides" (figure 4A). Each split has 13 similar splits with a distance=1, where one sample has switched sides, and 91 splits with distance=2.

The NormalGamma score is not strong enough to discriminate between the "true" split and neighboring splits, since the distribution of scores is very tight. However, we can assume that a gene is more likely to be assigned to the real biological split, and less likely to be associated with a split with a distance>0 from the real split. We also work under the assumption that a true biological "context" is likely to influence many genes, and therefore larger clusters are more biologically relevant.

We use these two assumptions in order to identify the real gene-split associations and remove irrelevant clusters.

The cluster merging algorithm is a iterative process. Each cycle identifies the largest cluster, its genes are removed from all its neighboring clusters, and the process iterates till no more clusters can be identified.

The steps are:

1. Each cluster is scored based on its overlap with its neighbors:

$$Score(cluster_x) = \sum_{i\ where\ Distance(Split_X, Split_i) \leq d} \#(Genes_{Cluster_x} \cap Genes_{Cluster_i})$$

   we used d=2.

2. We then choose the largest cluster, and remove its genes from all clusters with a distance<=d.

To save computing time, only clusters that enter the algorithm with 5 or more genes are allowed to be selected.

Step 3: Adding genes to remaining clusters

In the last step, after filtering most clusters out, we relax the statistical thresholds and add genes to the clusters (see Litvin et al 2009). We found this step to be necessary due to the small sample size, and the relatively high noise of gene expression data.

The thresholds used in this step are:

- Permutation pvalue<0.05.
- *NormalGamma* (right)+ *NormalGamma* (left)- *NormalGamma*(all samples)>0

*Code available on Pe'er lab's website (http://www.c2b2.columbia.edu/danapeerlab/html/).

Perturbation reveals patterns hidden in pre-perturbation data

To identify genes that are correlated only post- but not pre- perturbation we used a method similar to step 1 in COSPER. Specifically, we searched for clusters that show the behavior depicted in figure 2B, by associating genes to clusters only if they have a good score in post-perturbation data, but a bad score in steady state data.

We used stringent thresholds to define "good" and "bad" scores. The good score was defined as a permutation-based NormalGamma score < 0.01, and a bad score was with a permutation p-value > 0.5. Additionally, we require that a gene will be associated only if the post-perturbation NormalGamma score will demonstrate:

NormalGamma (right)+ *NormalGamma* (left)- *NormalGamma*(all samples)>0

While the pre-perturbation score will be:

NormalGamma (right)+ *NormalGamma* (left)- *NormalGamma*(all samples)<0

To remove spurious associations, we only considered clusters with > 20 genes. Overall, 3941 genes were associated with one or more clusters. As an example to this behavior, we show one such cluster in figure 2A.

COSPER results on steady-state or post-inhibition data alone

Combining pre- and post-inhibition data facilitates the identification of context-specific regulation and differential activation of pathways, while pre-inhibition data or steady state data alone fall short due to lower specificity and sensitivity.

We ran COSPER on each data set alone (pre or post inhibition). The number of modules increases dramatically, to 2684 with steady state data, and 1524 with post-inhibition data, compared with only 70 when using both data sets. Specificity is lost and those numbers make it much harder to analyze and interpret the results, while also increase the statistical burden for any post-analysis statistical tests.

Additionally, each cluster becomes much larger and less specific to MAPK targets. For example, STAT3 module contains 740 genes, compared with 28 genes using both datasets. While the later cluster is enriched for STAT3-related terms, the larger pre-inhibition cluster is enriched for *MITF* related annotations, although the one group of samples contains both *MITF*-positive (3) and *MITF*-negative (8) cell lines. The influence of MITF in melanoma is so strong (Principal component 1 is correlated with MITF and explain 30% of the variance), that by using only steady-state data all other signals become undetectable. Overall, the modules when running with steady state data alone are much larger, containing on average 194 genes compared with 33 when using the two datasets. This hampers power of many analysis tools, including LitVAn and gene set enrichment.

COSPER results on post-inhibition data alone are even less informative, with enrichments and biological coherence for both the STAT3 and STAT1 modules completely missing and we no longer have tight modules that can narrow down individual pathways. Instead we see general processes expected from inhibition of a key oncogenic pathway, such as cell cycle regulation, changes in metabolism, signal transduction, etc.

The combination of pre- and post-inhibition data, therefore, provides specificity and limits the cluster genes to only genes directly regulated by MAPK, while also provides the context of regulation.

Comparison of BRAF and MEK inhibition - PLX4720 vs. PD901

We used PD901 to inhibit the MAPK pathway, and not the more clinically used PLX4720 BRAF-V600E inhibitor to allow a direct comparison of BRAF and NRAS mutant cell lines. To ensure the short-term drug effects are similar, we compared the transcriptional response of MalMe3M, a BRAF-V600E cell line, following PD901 or PLX4720 treatment. We assessed expression fold change at 1 hour, 2, 4, and 8 hours following treatment using Illumina HumanHT-12 microarrays.

Preprocessing

Illumina's probe pvalues were used to filter out probes. Probes with p-value>0.05 in more than half of the samples were removed. Then microarrays were normalized according to their 75% percentile values. The 2 control array were averaged, and treated samples were compared to the averaged control to assess fold change.

Results

MEKi and BRAFi are remarkably the same at all time points. Although some probes were noisy, resulting in minor difference between treatments, no gene had a difference greater than 0.5 fold (on a log2 scale) between treatments at all time points. Only 6 probes, out of 16000, had a difference of more than 1 fold at 8 hour time point (figure S1B). None of them had such difference at 4 hours, suggesting that the difference arises from measurement noise.

We conclude that there is no difference in the short-time transcriptional response between treatments in this cell lines.

Comparison of the response to MEK inhibition between known genetic contexts

Both inactivation of PTEN and the type of MAPK activation (BRAF or NRAS) have been previously associated with the response to MAPK pathway inhibition. We examined

whether these mutations are correlated with the transcriptional response to MEK inhibition or the basal expression levels prior to MEK inhibition.

We used t-test to compare the expression levels between BRAF- and NRAS mutant cell lines (figure S2A), and between PTEN-null and PTEN-wild type cell lines (figure S2B). In both cases we found that no genes are associated with those genetic contexts (FDR q-value < 0.05), either before of after pathway inhibition.

PD901 and IFNβ microarray results

Data Preprocessing

Six cell lines were chosen for analysis. 3 are low-pSTAT1 – A375, SkMel133 and SkMel2, and 3 high-pSTAT1 – SkMel105, SkMel39 and WM1361. They were treated with 50nM PD901, 1000U/mL IFNβ or their combination. Samples were collected 8 hours after treatment, control samples were collected at 0h. RNA extraction, labeling and hybridization were conducted as described under methods. Agilent human 8x60 gene expression arrays were used.

Raw data normalization and filtering were conducted as described above, with a low threshold of 7, and an upper threshold of 17.5.

IFN response in high- vs. low- pSTAT1 cell lines

The IFN response includes dozens of genes with a dramatic induction in gene expression, of up to 500 fold, in all 6 cell lines (figure S5B).

There is, however, a difference in the extent of change in high- vs. low- pSTAT1 cell lines, that can be attributed to the different basal expression level of those genes (data not shown). The maximum level of expression seems to be similar in all cell lines, but high pSTAT1 cell lines have a higher basal activity and therefore the fold change is lower.

In order to compare the activation of the pathway between the two cell line groups, it is better to use the final expression level, i.e. the basal expression+fold change. However, such comparison reveals the expression of no genes is statistically significant different between high- and low-pSTAT1 cell lines (using t-test and FDR correction).

We therefore determine that there is no difference in the response to IFNβ between high- and low-pSTAT1 cell lines.

Combinatorial treatment and synergy

To test whether the MEK inhibition and IFNβ synergize at the level of gene expression, we compared the fold change of the dual treatment with that of MEKi+IFNβ as single agents. Over all, those responses are very similar (figure S5C).

If no synergy exists, the values of Both-(MEKi+IFNβ) should be close to 0. Only one gene significantly deviates from 0 in all 6 cell lines. The gene is CCL4, and it is induced both by MEKi and IFNβ treatment as single agents, but a combinatorial treatment isn't additive.

We couldn't identify any other genes that show a synergetic response in all 6 cell lines, or separately in low- or high-pSTAT1 lines (we defined synergy is the equation above >1 or <-1).

MITF binding site analysis

To assess frequency of MITF binding site in gene promoters we used the motif CACATG, known to be a target sequence of MITF. Gene promoters were defined as 5000bp upstream of their transcription start site, or up to the closest upstream gene, whichever is shorter. For each gene, number of binding motif in its promoter sequence was noted.

To assess the significance of number of motif occurrences, we used the binomial distribution. Since the MITF-M and *MITF*-expression clusters are similar and share genes, for the purpose of this analysis genes were assigned to only one of the clusters based on their NormalGamma score. For each one of the two clusters, MITF-M and *MITF*-expression, we counted total number of motif occurrences in all the cluster genes. For simplicity, the expected probability of the motif to randomly appear in a DNA sequence is $2 * 1/4^6$ (6 is the length of the motif, and 2 represent the two strands).

The pvalue of X occurrences is the probability of randomly observing X or more occurrences in a random sequence, or 1-BINOMIAL_CDF(X, N, p), where N is total sequence length and p is $2/4^6$.

For MITF-M cluster, the total promoter sequence is 120735bp, with 83 motif occurrences (59 expected). For *MITF*-expression cluster, the total promoter sequence is 183399bp, with 86 occurrences (89 expected).

Cytochrome C release

Protocol for Cytochrome C release is taken, as is, from Majewski et al 2004. It is brought here for convenience:

Lysis buffer: 20 mM Hepes-KOH, [pH 7.5], 210 mM sucrose, and 70 mM mannitol; 1.5 mM MgCl2, 10 mM KCl2, protease inhibitor, and 1 mg digitonin/1mL lysis buffer.

Cells are trypsinized, collected and spun down in 4C. They are then washed with PBS and spun down again. It is critical that cell pellets will be lysed immediately without freezing.

Cells are gently suspended, without vortexing, in lysis buffer. Roughly double the cell pellet volume is used. They are incubated in 25C for 3-10min, depending all cell line. Spun down at 4C for 20 minutes at highest speed. Supernatant contains cytoplasmic fraction.

Protein concentration was assessed using BCA.

Fluorescent Microscopy

Cells were plated onto Corning BioCoat Poly-D-Lysine glass 8-well culture slide (Corning 354632) at a density of 15,000 to 40,000 cells/well and allowed to attach to the surface for 24 hours. Cells were then treated with 50 nM PD0325901, and the same volume of DMSO was added to controls at the time of treatment.

CytoC released was measured 30 hours after treatment. Cells were washed 1X with PBS, fixed with 4% PFA in PBS for 10 min at room temperature, and washed 2X with PBS (5 min / wash). Cells were then blocked and permeabilized in 5% BSA/0.3% TX-100 in PBS for 1 hr at room temperature.

Cells were incubated with Anti-Cytochrome C antibody (Abcam ab110325) at 1 µg/mL in 1% BSA/0.1% Tween-20 in PBS overnight at 4 °C, when washed 3X with 1% BSA/0.1% Tween-20 in PBS (5 min / wash), and then incubated with Alexa Fluor 488 Goat Anti-Mouse IgG2a (γ2a) (Molecular Probes A-21131) at 1 µg/mL in 1% BSA/0.1% Tween-20 in PBS for 45 min in the dark at room temperature. Cells were washed 3X with 1% BSA/0.1% Tween-20 in PBS (5 min / wash).

Cells then were counterstained with NucBlue Fixed Cell ReadyProbes Reagent (Molecular Probes R37606) for 10 min, and washed in 2X with PBS (5 min / wash).

Slides were mounted with Fluoro-Gel with Tris Buffer (Electron Microscopy Sciences17985-10), and images were acquired using an inverted microscope (Nikon Eclipse TE2000-E) equiped with a 40X lens and illuminated with a mercury vapor short arc lamp (Olympus X-Ctie 120PC).

References

DeGroot, M.H. (2004). Optimal statistical decisions, Wiley classics library edn (Hoboken, N.J.: Wiley-Interscience).

Litvin, O., Causton, H.C., Chen, B.J., and Pe'er, D. (2009). Modularity and interactions in the genetics of gene expression. Proceedings of the National Academy of Sciences of the United States of America *106*, 6441-6446.

Segal, E., Shapira, M., Regev, A., Pe'er, D., Botstein, D., Koller, D., and Friedman, N. (2003). Module networks: identifying regulatory modules and their condition-specific regulators from gene expression data. Nature genetics *34*, 166-176.